Synthesis, Characterization, Chemical Reduction and Biological Application of Graphene Oxide

by

Xiguang Gao

A thesis

presented to the University of Waterloo

in fulfillment of the

thesis requirement for the degree of

Master of Science

in

Chemistry - Nanotechnology

Waterloo, Ontario, Canada, 2013

Author's Declaration

I hereby declare that I am the sole author of this thesis. This is a true copy of the thesis, including any required final revisions, as accepted by my examiners.

I understand that my thesis may be made electronically available to the public.

Abstract

As an atomic layer of sp^2-hybridized carbon atoms closely packed in a honeycomb lattice, graphene has been attracting increasing attention since its discovery in 2004 due to its extraordinary physicochemical properties. Graphene oxide (GO), a non-stoichiometric graphene derivative with the carbon plane abundantly decorated with hydroxyl, epoxide and carboxylic groups, can be massively and cost-effectively produced from natural graphite following Hummers method. GO has greater aqueous solubility than pristine graphene due to its oxygen-functionalities. Various solution-based chemical methods can be applied to GO, which has stimulated a new research area called 'wet chemistry of grahene'. Among them, chemical reduction of GO provides a facile route for large-scale synthesis of graphene.

With abundant oxygen-functionalities in its structure, GO can potentially act as a suitable precursor for chemical modifications of graphene through methods used in organic chemistry. Special attention should be paid to that the hydroxyl groups in GO belong to tertiary alcohols, and steric hindrance should be considered when performing chemical modifications. Diethylaminosulfur trifluoride (DAST), a fluorinating reagent, is ineffective in fluorinating GO due to the steric hindrance of tertiary hydroxyls. However, DAST is effective in reducing GO. The capability of DAST for GO reduction is close to hydrazine, but the reduction reaction can be performed at lower temperature for DAST.

As a two-dimensional (2D) nanomaterial with good aqueous solubility, biocompatibility and excellent intrinsic mechanical properties, GO is particularly useful in preparing 3D hybrid hydrogel scaffolds for tissue engineering applications.

Acknowledgements

First of all, I would like to sincerely thank my supervisor Prof. Xiaowu (Shirley) Tang for her guidance and support during my Master study! Discussing with her about the experimental results benefited my research a lot. Her broad range of knowledge enables her to give me insightful ideas and suggestions about research. I made steady progress under her supervision.

Second, I want to thank my parents who have brought me up and educated me! They can always cheer me up whenever I feel down. I gain self-confidence and positive energy from them.

Third, I want to thank all my colleagues in the Tang lab! Their hard-working and keen attitudes towards research really encouraged me. They have created a wonderful atmosphere for me to conduct research. They helped me a lot as well.

I also want to thank the Department of Chemistry at University of Waterloo for accepting me as a graduate student and providing me with funding! I had such a great time studying and working here. This experience will be a treasure to both of my life and future career.

Finally, I want to thank all the people who have helped me toward this stage of my life!

Table of Contents

List of Figures

List of Tables

List of Equations

List of Abbreviations

2D: two-dimensional

FET: field effect transistor

AFM: atomic force microscopy

CVD: chemical vapor deposition

GO: graphene oxide

rGO: reduced graphene oxide

CCG: chemically converted graphene

TBA: tetrabutylammonium hydroxide

DSPE-mPEG: 1,2-distearoyl-sn-glycero-3-phosphoethanolamine-N-[methoxy(polyethylene-glycol)-5000]

TEM: transmission electron microscopy

GNRs: graphene nanoribbons

STM: scanning tunneling microscopy

QHE: quantum hall effect

FG: fluorinated graphene

DAST: diethylaminosulfur trifluoride

FTIR: Fourier transform infrared spectroscopy

UV-Vis: ultraviolet visible spectroscopy

SEM: scanning electron microscopy

XPS: X-ray photoelectron microscopy

GICs: graphite intercalation compounds

XRD: X-ray diffraction

GelMA: gelatin methacrylate

FITC: fluorescein isothiocyanate

MeGO: methacrylic graphene oxide

Chapter 1 - Introduction

1.1 The Discoveries of Graphene as Well as Other Quasi Two Dimensional (2D) Materials

The term graphene was first introduced by Boehm *et al.* in 1986 and derived from the combination of the word 'graphite' and the suffix 'ene' that refers to polycyclic aromatic hydrocarbons (e.g. anthracene, benzene).[1,2] However, free-standing graphene crystal was not discovered until 2004 when Dr. Andre K. Geim and Dr. Konstantin S. Novoselov from the University of Manchester successfully peeled off highly ordered pyrolytic graphite (HOPG) and obtained single layer graphene crystal using the 'Scotch Tape' method.[3] Afterwards, they also obtained other atomic 2D crystals including BN, MoS_2, $NbSe_2$ and $Bi_2Sr_2CaCu_2O_x$ using the same technique.[4] The researches on graphene and other 2D materials have intensively expanded ever since.[5-8] The Nobel Prize in Physics 2010 was awarded jointly to Andre Geim and Konstantin Novoselov "for groundbreaking experiments regarding the two-dimensional material graphene".[9]

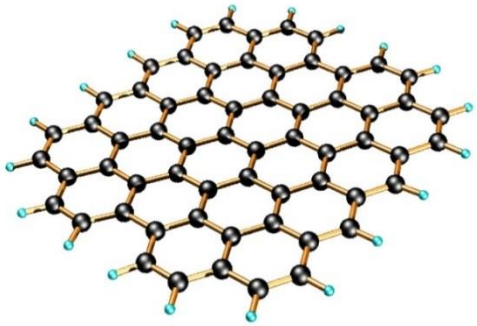

Fig. 1 Schematic of the structure of graphene.[10]

Schematic of the structure of graphene is shown in Fig. 1. It can be seen as a single layer of sp^2-hybridized carbon atoms closely packed in a honeycomb crystal lattice. Every carbon

atom in graphene is covalently bonded to three adjacent carbon atoms. The large π network across the molecular chicken wires contributes to its excellent electrical properties. Graphene is a building block for other carbon-based materials. It can be wrapped up into 0D fullerene, rolled into 1D carbon nanotubes and stacked into 3D graphite.[11]

Graphene has stimulated tremendous research interests among other 2D materials since its advent due to its extraordinary physicochemical properties. Graphene has remarkably high charge carrier mobility in excess of 15,000 $cm^2 V^{-1} s^{-1}$ under ambient conditions,[11] excellent thermal conductivity of ~5000 $Wm^{-1}K^{-1}$ at room temperature,[12] Young's modulus of 1.0 TPa,[13] optical transmittance of 97.7%,[14] high theoretical specific surface area of 2630 m^2g^{-1}. And graphene is chemically stable under ambient conditions. Graphene has a wide range of applications including field effect transistors (FETs),[15] gas sensors,[16] nanocomposite materials[17] and supercapacitors[18] due to its excellent physicochemical properties.

1.2 Graphene Synthesis

1.2.1 Scotch Tape Method (Micromechanical Cleavage of Graphite)

Scotch Tape method or micromechanical cleavage of graphite led to the discovery of graphene in 2004. This method involves repeatedly peeling highly oriented pyrolytic graphite (HOPG) using a scotch tape, transferring graphene as well as thick graphite flakes onto a Si substrate with a SiO_2 layer of a carefully chosen thickness (300 nm), and hunting graphene under an optical microscope. Schematic of this method is shown in Fig. 2. An atomic force microscopy (AFM) image of a graphene crystal produced by this method is shown in Fig. 3.

The thickness of graphene was measured to be 0.4 nm by AFM, which is close to its theoretical value of 0.34 nm.[19]

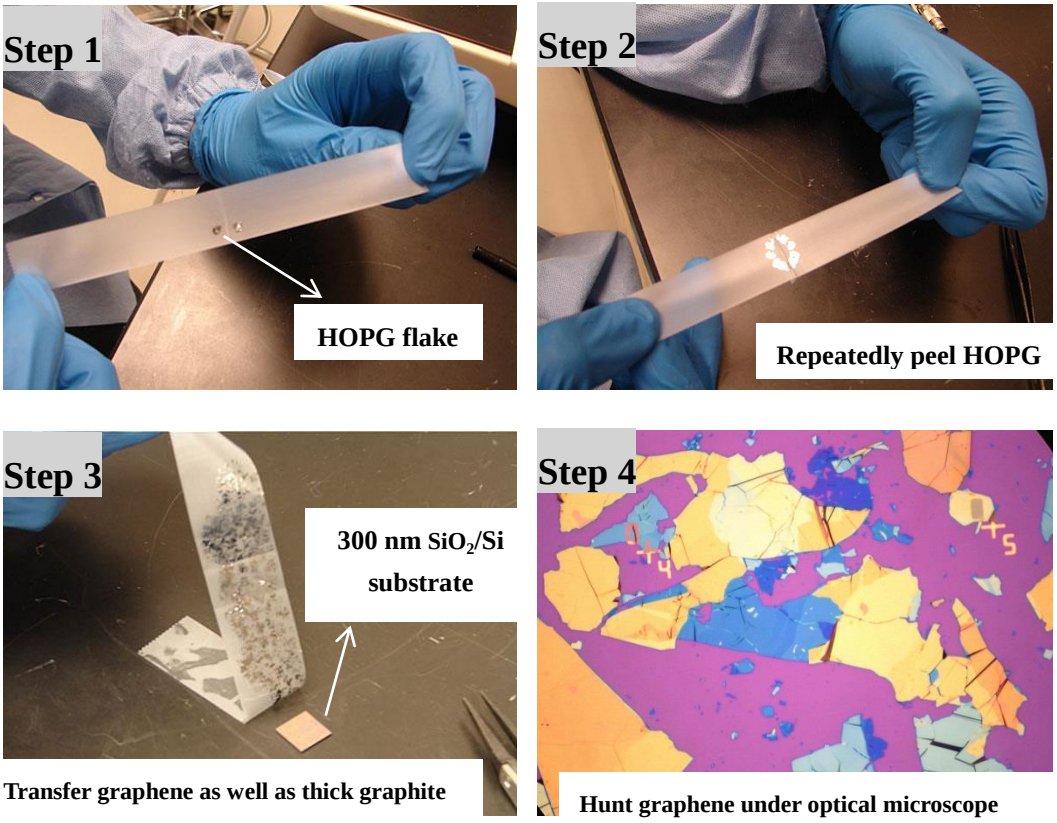

Fig. 2 Schematic of the Scotch-Tape method.[19]

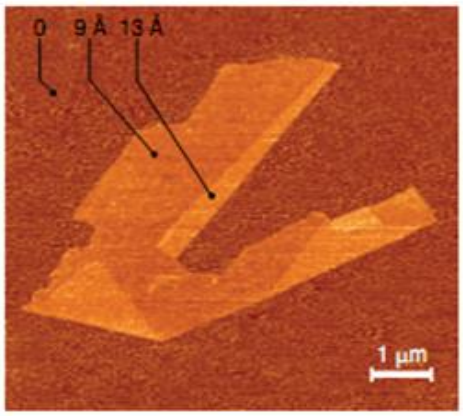

Fig. 3 AFM image of a graphene crystal obtained by Scotch Tape method. The folded region exhibiting a relative height of 4 Å indicates it is single layer. (Adapted with permission from ref. 11. © 2007 Nature Publishing Group.)

Peeling HOPG with an adhesive tape is a commonly used technique to prepare freshly cleaved surfaces for depositing samples in AFM characterization. The peeled graphite flakes have a wide range of thicknesses. Breakthrough in getting single layer graphene did not come until the use of a Si wafer with a carefully chosen thickness of SiO_2 layer which makes graphene visible under an optical microscope. Single layer graphene, few layer graphene and thicker graphite flakes show different colors on a 300-nm-thick SiO_2/Si substrate due to feeble interference-like contrasts with respect to an empty substrate.[4]

This method can provide high quality graphene crystal with lateral size up to 100 μm, however, it is laborious and the yield is very low, rendering this method unsuitable for large scale production of graphene.

1.2.2 Epitaxial Growth on Silicon Carbide (SiC)

Graphitization of silicon carbide by Si sublimation under high temperature and vacuum conditions was first reported in the 1960s.[20] Berger *et al.* have refined this technique and demonstrated that patterned epitaxial graphene grown on single SiC crystal showed electronic confinement and coherence, which envisages coherent graphene molecular electronics. [21, 22] Lin *et al.* reported that FETs fabricated on wafer-scale epitaxial graphene exhibited high cutoff frequency of 100 GHz which exceeded Si/metal-oxide semiconductor FETs, demonstrating the high potential of epitaxial graphene grown on SiC for electronic applications.[15]

Epitaxial growth on SiC has been one of the leading methods for mass-production of graphene. However, growing large graphene domains and sophisticated control over the

thickness of the graphene film remain as major challenges so far. The high growth temperature (1200 ℃~1800 ℃), high cost of SiC substrates, ultrahigh vacuum condition (UHV) and non-transferability of as-grown graphene films to arbitrary substrates are the disadvantages of this method.

1.2.3 Chemical Vapor Deposition (CVD) on Transition Metals

The syntheses of graphitic materials (e.g. carbon nanotubes) by chemical vapor deposition on transition metals (e.g. Fe, Co, Ni, Cu, Ru, Pd) have a long history. Different from using transition metal nanoparticles for growing carbon nanotubes, transition metal thin films are normally used for growing graphene films. Large-scale patterned growth of few layer graphene films on thin Ni films were realized by Kim *et al.*[23] The as-grown graphene films could be easily transferred to arbitrary substrates. The transferred graphene films showed low sheet resistance of 280 Ω per square at 80% optical transparency. At low temperatures, monolayer graphene transferred to SiO_2 substrates showed electron mobility greater than 3,700 $cm^2\ V^{-1}\ s^{-1}$ and exhibited the half-integer quantum Hall effect (QHE), implying that the quality of CVD-grown graphene on Ni is comparable to graphene obtained by mechanically cleavage of graphite.

However, as the carbon solubility in Ni is relatively high (1.2 at% at 1000 ℃), controlled growth of exact monolayer graphene is difficult. When carbon species start precipitating out from the surfaces of Ni films, multilayer graphene or graphite can be formed along with monolayer graphene. Graphene films grown on Ni usually do not possess uniform thicknesses, which limits their application in electronics. In order to prevent the formation of multi-layer

graphene, fast cooling rate (~10 ℃ s^{-1}), thin Ni films (<300 nm), and/or extremely low concentration of carbon source are usually required for growing monolayer graphene.[23-24] Cu has a much lower carbon solubility (less than 0.004 at% at 1000 ℃) than Ni, making it a better candidate for making strict monolayer graphene by CVD. Li *et al.*[25] reported the large-area synthesis of high-quality and uniform graphene films on copper foils and concluded that graphene growth on Cu is a surface-catalyzed and self-limiting process rather than an absorption-precipitation process proposed for Ni. Graphene grown on Cu showed electron mobility as high as 4,050 cm^2 V^{-1} s^{-1} at room temperature. Fig. 4a shows the graphene films transferred on a glass substrate grown by CVD Cu. The area of the film is ~1.2 cm×1.0 cm. Fig 4b shows the optical image of graphene films transferred on a 285-nm-thick SiO_2/Si substrate. Graphene of different layers show different light contrasts with the substrate. The films consist of predominantly single layer graphene with a percentage of >95%.

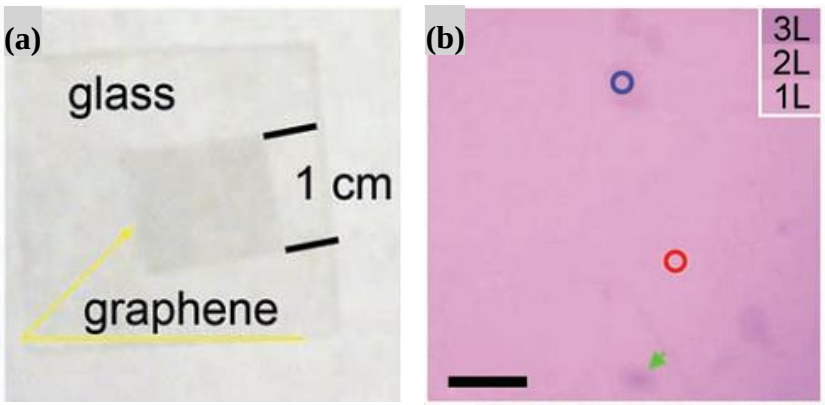

Fig. 4 (a) Graphene films transferred onto a glass substrate, (b) Optical microscope image of graphene films transferred onto a 285-nm-thick SiO_2/Si substrate. (Adapted with permission from ref. 25. © 2009 AAAS.)

By using CVD on flexible wrapped-up copper foils, Bae *et al.* synthesized a 30-inch predominantly monolayer graphene film (Fig. 5).[26] The flexibilities of graphene films and copper foils allowed efficient transfer process using a roll-to-roll method. The scalability of CVD on Cu for large-scale graphene synthesis was well illustrated in this work.

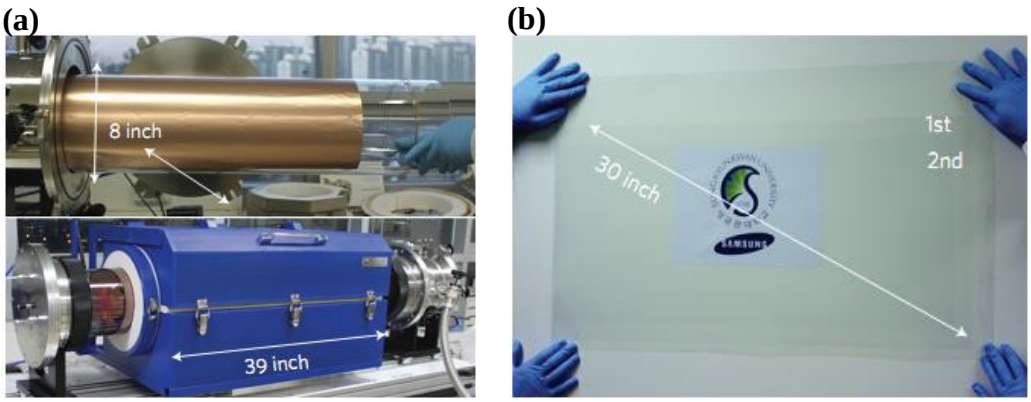

Fig. 5 (a) Copper foil wrapping around a 7.5-inch quartz tube was inserted into an 8-inch quartz reactor, (b) a transparent ultralarge-area graphene film (30 inches) transferred on a 35-inch polyethylene terephthalate (PET) substrate. (Adapted with permission from ref. 26. © 2010 Nature Publishing Group.)

CVD on transition metals (Ni, Cu) can produce high-quality graphene and are suitable for large-scale synthesis. However, high temperature heating (normally 1000 ℃), low pressure growth condition in case Cu is used, and transfer of graphene films to other substrates are required, making this method not very cost-effective and facile.

1.2.4 Chemical Reduction of Graphene Oxide (GO)

The synthesis of graphite oxide can date back to as early as 1859. British chemist Brodie first explored the reaction of graphite with potassium chlorate ($KClO_3$) in fuming nitric acid (HNO_3), and synthesized "graphitic acid" (graphite oxide) with a net molecular formula of $C_{2.19}H_{0.80}O_{1.00}$ by successive oxidation processes (four reactions).[27] Later in 1898,

Staudenmaier improved Brodie's method by adding $KClO_3$ in multiple aliquots in the course of the reaction and using concentrated sulfuric acid in addition to nitric acid.[28] This method was more convenient compared with Brodie's multiple reactions and resulted in graphite oxide with a C/O atomic ratio of 2.89:1. In 1958, Hummers and Offeman developed an alternate oxidation method to prepare graphite oxide by reacting graphite with potassium permanganate ($KMnO_4$) in concentrated sulfuric acid and sodium nitrate ($NaNO_3$).[29] The resulting graphite oxide has a C/O ratio of 2.25:1.

The structure of graphite oxide:

The reactions of graphite with oxidants ($KClO_3$ or $KMnO_4$) in concentrated sulfuric acid and nitric acid are complicated and the precise reaction pathways are unknown so far. The exact chemical structure of graphite oxide is also unknown as a result. However, there are some structure models depicting it, e.g. Hofmann model,[30] Ruess model,[31] Scholz and Boehm model,[32] Lerf and Klinowski model.[33] Among them, the Lerf and Klinowski model is the most widely accepted.

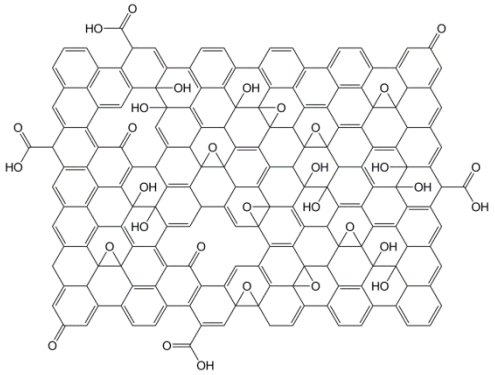

Fig. 6 Schematic of the structure of graphite oxide.

According to the Lerf-Klinowski model, the majority of oxygen-functional groups in graphene oxide are epoxide and tertiary hydroxyl groups which are located in the middle of the graphene plane, while small amount of carboxylic and/or carbonyl groups are located on

the edges. A schematic of the structure of graphite oxide according to this model is shown in Fig. 6. Recently Gao *et al.* showed evidences for the presences of five- and six-membered-ring lactols (not shown in Fig. 6) in graphite oxide by solid state ^{13}C nuclear magnetic resonance (NMR) characterization.[34]

Graphite oxide can be easily dispersed in water and exfoliated into single-layered graphene oxide by ultrasonication.[35] The synthesis of graphene oxide from graphite is cost-effective and scalable for mass production. While graphene oxide is insulating, its deoxygenation by chemical reducing agents can restore the conductivity and produce the so-called reduced graphene oxide (rGO) or chemically converted graphene (CCG). A myriad of reductants have been developed up to now, including sodium borohydride,[36-37] hydrazine,[35,38-39] hydroquinone,[40] strong base (KOH or NaOH),[41] hydriodic acid (HI),[42-43] alumina powder,[44] L-ascorbic acid,[45] vitamin C,[46] benzyl alcohol,[47] zinc/sulfuric acid (Zn/H_2SO_4),[48] lithium aluminum hydride ($LiAlH_4$).[49] Among them hydrazine (N_2H_4) and hydriodic acid (HI) are the most commonly used ones.

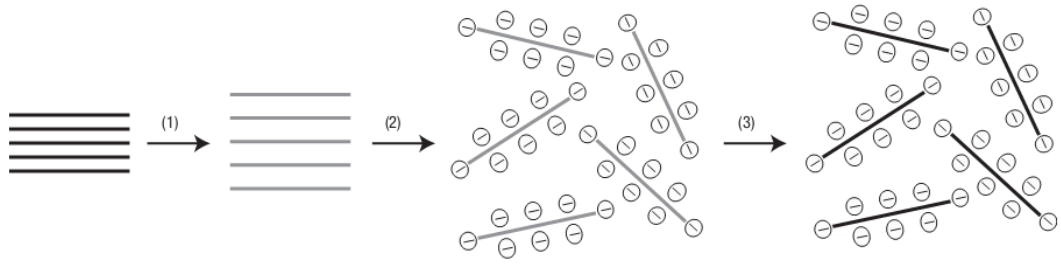

Fig. 7 Scheme showing the chemical reduction of graphene oxide to produce aqueous graphene solution. (Adapted with permission from ref. 38. © 2008 Nature Publishing Group.)

Fig. 7 shows the schematic of chemical reduction of graphene oxide for the production of graphene aqueous solution. Step 1 is oxidation of graphite (black blocks) to graphite oxide

(lighter colored blocks) with larger interlayer distance. Step 2 is exfoliation of graphite oxide in water by sonication to obtain graphene oxide colloids that are stabilized by electrostatic repulsion. Step 3 is controlled conversion of graphene oxide colloids to conducting graphene colloids by hydrazine reduction at pH=10.[38]

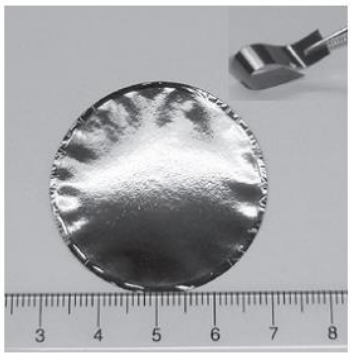

Fig. 8 Photograph of a 10-μm-thick chemically converted graphene (CCG) film (diameter ~38 mm) prepared by vacuum filtration of a CCG colloid. The inset image shows a strip of this film is bendable. (Adapted with permission from ref. 38. © 2008 Nature Publishing Group.)

Photograph of a chemically converted graphene (CCG) film (thickness ~10 μm, diameter ~38 mm) prepared by vacuum filtration of the resulting graphene colloid is shown in Fig. 8. The film exhibited shiny metallic luster with flexibility. The conductivity of the film measured by a four-probe method was 7,200 S m^{-1}. The highest values reported for C/O atomic ratio and conductivity of rGO by hydrazine reduction are ~9.97 and ~7,200 S m^{-1}, respectively, while those values of rGO by HI reduction are 15. 27 and 30,400 S m^{-1}, respectively.[38,42]

The mechanism for graphene oxide reduction by hydrazine is unknown so far. However, it is generally accepted that hydrazine reduction leads to the incorporation of a small amount of nitrogen (1.0 at%~3.0 at%) into the structure of rGO.[50] The incorporation of nitrogen is

probably through the formation of pyrazoline structure at the edges of graphene platelet which can evolve into pyrazole structure under thermal annealing, leading to the generation of aromatic nitrogen doping as shown in Fig. 9.[51]

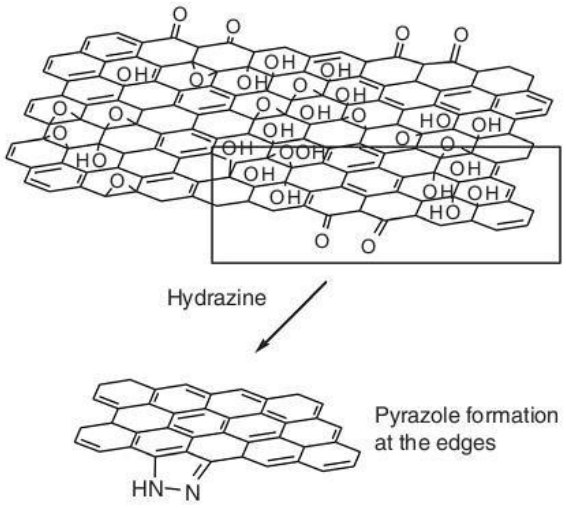

Fig. 9 Schematic illustrating the formation of pyrazole structure at the graphene platelet edges by hydrazine reduction. (Adapted with permission from ref. 51. © 2012 Nature Publishing Group.)

The precise mechanism for graphene oxide reduction by HI is also unknown. Possible reduction pathways are shown in Fig. 10. Since iodine ion (I^-) is a well-known strong nucleophile, I^- can attack the epoxide and hydroxyl groups in graphene oxide and lead to the formation of C-I intermediate, in other words, nucleophile substitutions of epoxide and hydroxyl groups by iodine. However, iodine is eventually eliminated from the C-I intermediate with the formation of new C=C bonds meanwhile as C-I bond is not thermodynamically favored. The reduction by HI can be viewed as an iodine-ion-catalyzed reaction.

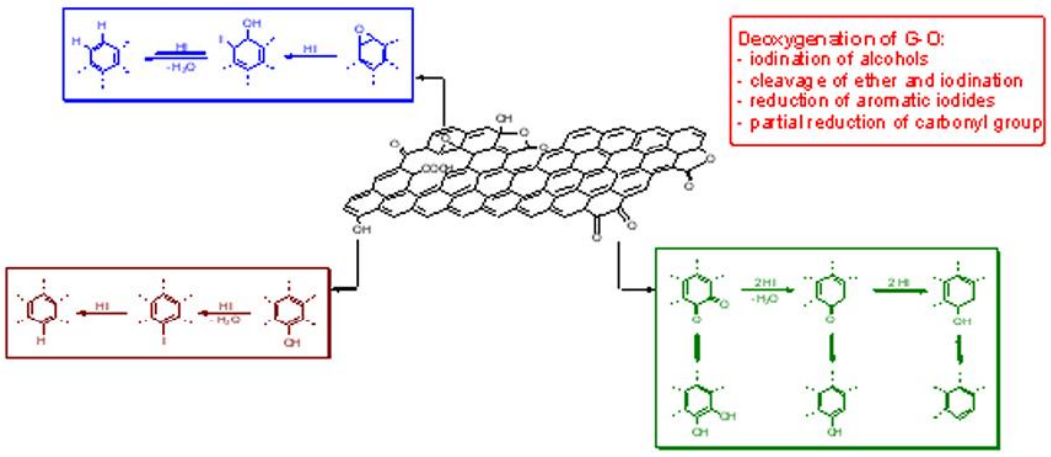

Fig. 10 Schematic showing possible mechanism for graphene oxide reduction by HI. (Adapted with permission from ref. 42. © 2010 Nature Publishing Group.)

Chemical reduction of graphene oxide for graphene synthesis is a solution-based method which is suitable for mass production. It is particularly advantageous over other methods in the areas of large-area transparent conductive films (TCFs) for electronics simply by spin-coating to deposit ultrathin graphene oxide films first followed by chemical reduction, graphene-metal-oxide composites for supercapacitors and lithium ion batteries, and graphene-polymer composites.[52-54,17] Moreover, free-standing graphene film with thickness in the range of micrometer can be prepared by vacuum filtration a graphene solution. Last but not least, it is facile and cost-effective. The temperature needed for synthesizing and reducing graphene oxide is relatively low (<100 ℃) which is in stark contrast to the high temperature (~1000 ℃) needed for the CVD method.

However, the disadvantage of this method is that the electrical property of rGO is not as good as that of graphene obtained by CVD or scotch tape method. The severe oxidation of graphite creates many defects in the structure of carbon plane, which cannot be repaired by

chemical reduction. The large D band with respect to the G band, the broadening of the G band and the disappearance of the 2D band in the Raman spectrum of rGO[42] reveal that rGO has many defects (holes or vacancies) existing in its structure and is different from graphene obtained by CVD or scotch tape method. Chemical reduction of graphene oxide can restore the π-networks and make it conductive, but cannot repair the defects in graphene oxide.

1.2.5 Sonication-Assisted Exfoliation of Graphite in Organic Solvents

Exfoliation of graphite by sonication in organic solvents with or without surfactants was first reported by Dai's group and Coleman's group in 2008.

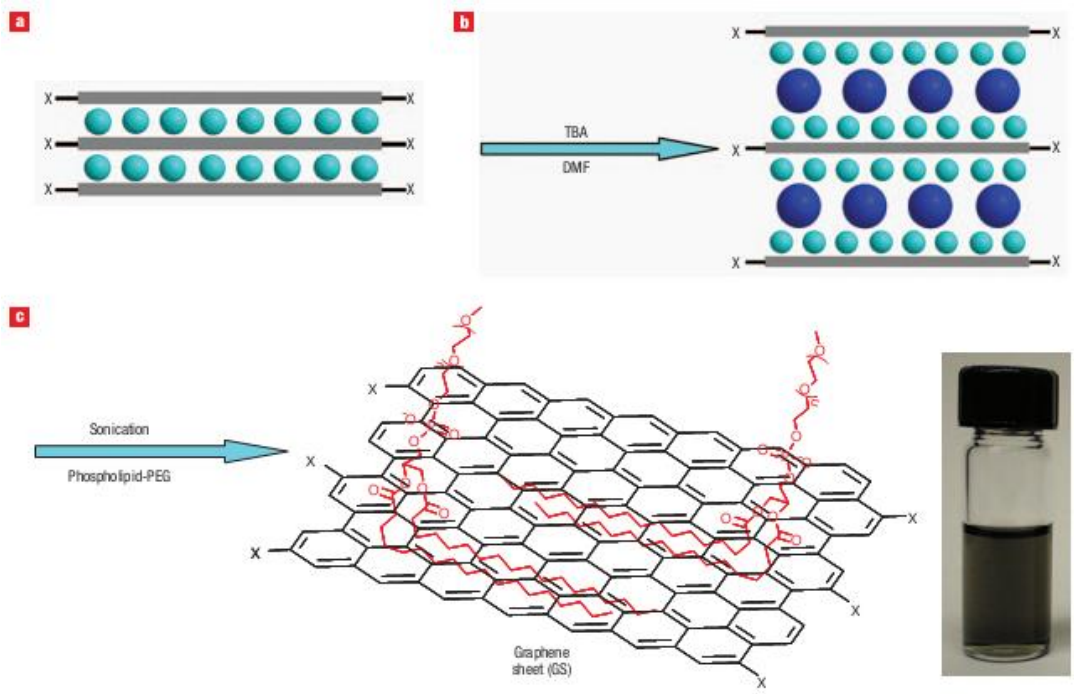

Fig. 11 Schematic showing the sonication-assisted exfoliation of graphite. (a) Intercalating graphite with sulfuric acid molecules (teal spheres), (b) inserting TBA (blue spheres), (c) sonication of TBA-inserted-sulfuric-acid-intercalated graphite with DSPE-mPEG. A photograph of an as-produced DSPE-mPEG/DMF solution of graphene sheets is also shown. (Adapted with permission from ref. 55. © 2008 Nature Publishing Group.)

Dai's group obtained high-quality graphene sheets by briefly heating commercial expandable graphite at 1,000 ℃ to exfoliate it first, reintercalating the exfoliated graphite with oleum, then inserting tetrabutylammonium hydroxide (TBA) molecules into the intercalated graphite, finally sonicating the TBA-inserted-oleum-intercalated graphite with 1,2-distearoyl-sn-glycero-3-phosphoethanolamine-N-[methoxy(polyethylene-glycol)-5000] (DSPE-mPEG). Schematic of the whole process is shown in Fig. 11. The as-produced graphene sheet had a resistance of 10-30 kΩ at room temperature which was 1,000 times lower than thermally reduced graphene oxide (800 ℃ in H_2 atmosphere) with a resistance of 20 MPa. And the resistance of as-produced graphene sheet showed only a small drop at low temperature indicating its quality was comparable to the peel-off pristine graphene.[55]

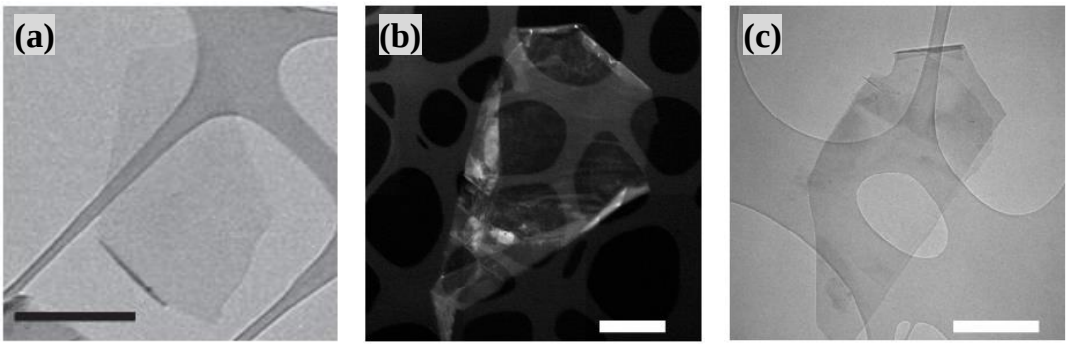

Fig. 12 (a) Bright-field and (b) dark-field TEM images of monolayer graphene, (c) bright-field TEM image of bilayer graphene. Scale bars are all 500 nm. (Adapted with permission from ref. 56. © 2008 Nature Publishing Group.)

Coleman's group exfoliated graphite to sub-five-layer graphene by sonication of graphite in organic solvents.[56] According to their theory, it is possible to exfoliate graphite to graphene when the energy cost is balanced by the solvent–graphene interaction for solvents whose surface energies match that of graphene. Such organic solvents suitable for graphite

exfoliation have surface tensions in the region of 40-50 mJ m^{-2}, e.g. benzyl benzoate, 1-methyl-2-pyrrolidinone (NMP), γ-butyrolactone (GBL), N,N- dimethylacetamide (DMA), 1,3-dimethyl-2-imidaz-olidinone (DMEU). Some typical transmission electron microscopy (TEM) images of graphene flakes obtained by sonication of graphite in NMP are shown in Fig. 12. A thin graphene film made by vacuum filtration of a graphene NMP solution showed a conductivity of ~6,500 S m^{-1} which is close to rGO by hydrazine reduction at pH=10 (conductivity ~7,200 S m^{-1}).

Sonication-assisted direct exfoliation of graphite in organic solvents is advantageous in making high quality graphene sheets which are much less defective than chemically or thermally reduced graphene oxide. However, the concentration of as-produced graphene sheet in organic solvent is very low (~0.01 mg/mL) which limits its applications. Yet removing the organic solvent or surfactant in case that surfactant is used is annoying. Coleman's group pointed out that an air-dried graphene thin film prepared by vacuum filtration of a graphene NMP solution contained ~11 wt% residual NMP as determined by X-ray photoelectron spectroscopy (XPS), and this value remained unchanged after a subsequent vacuum annealing at 400 ℃.[56]

1.2.6 Bottom-Up Synthesis

Cai *et al.*[57] reported the synthesis of atomically precise graphene nanoribbons (GNRs) by a bottom-up way. This method involved the use of surface-assisted coupling of molecular precursors into linear polyphenylenes and their subsequent cyclodehydrogenation. The reaction schemes and some typical scanning tunneling microscopy (STM) images are shown in Fig. 13. The

calculated bandgap for an N=7 armchair GNR (Fig. 13a) was 1.6 eV. Moreover, GNR heterojunctions could be created by heteromolecular coupling as shown in Fig. 13e.

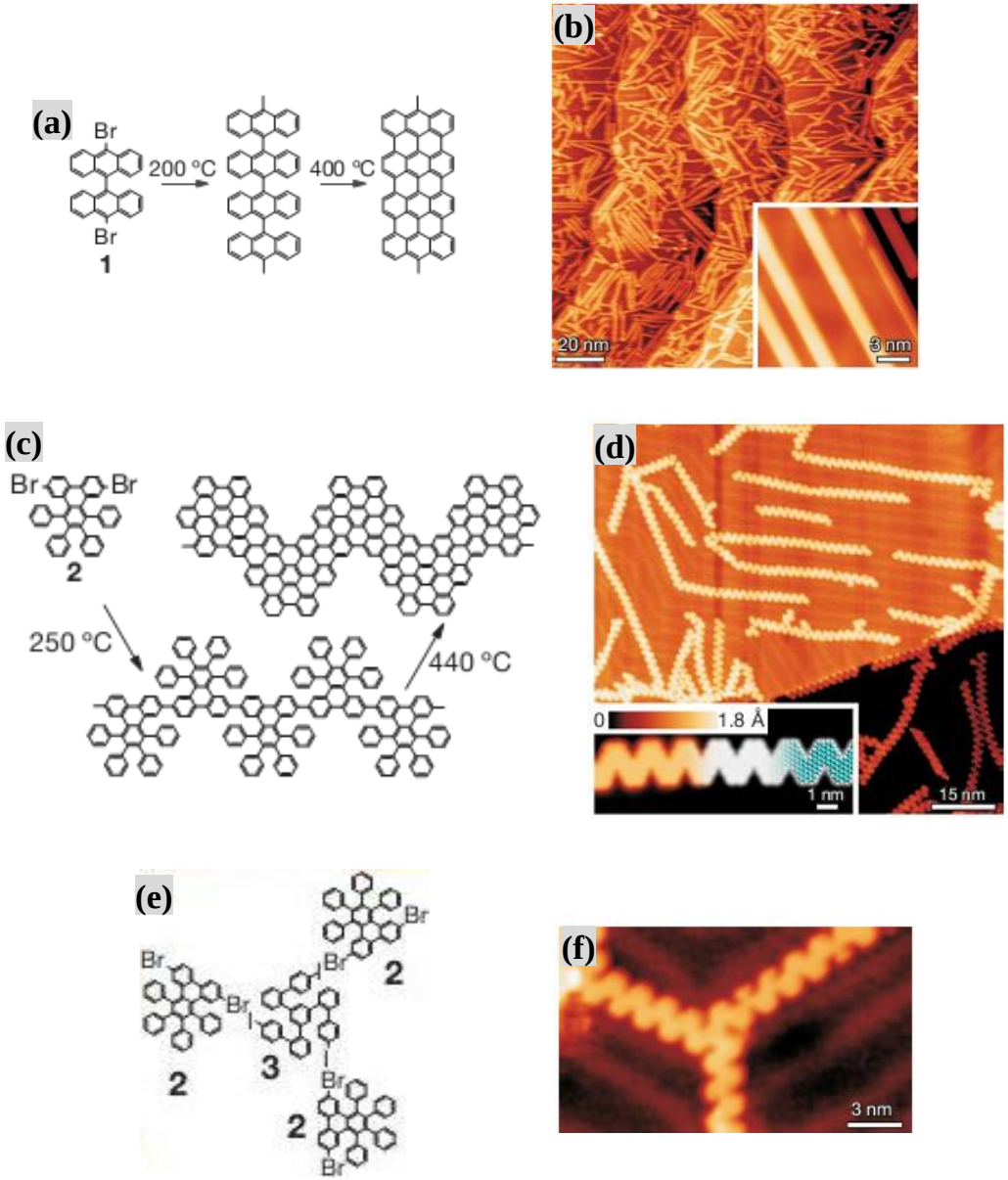

Fig. 13 Reaction schemes and STM images of GNRs. (a) Reaction scheme for synthesizing armchair GNR from precursor monomer **1**. (b) STM image of armchair GNRs. (c) Reaction scheme for synthesizing chevron-type GNRs from monomer **2**. (d) STM image of chevron-type GNRs. (e) Heteromolecular coupling between monomer **2** and **3**. (f) STM image showing the threefold GNR junction. (Adapted with permission from ref. 57. © 2010 Nature Publishing Group.)

The first step during the bottom-up synthesis of GNRs is the thermal sublimation of monomers on Au(111) or Ag (111) surfaces which results in some surface-stabilized biradical species, then the biradical species diffuse across the surface and undergo radical addition to form linear polymer chains. The second step is formation of aromatic GNRs through surface-assisted cyclodehydrogenation.[57] This method can produce GNRs at a modest temperature (<450 ℃), however, a suitable technique for transferring as-synthesized GNRs onto SiO_2 substrates for electronics needs to be developed. Yet the electrical properties of as-synthesized GNR are open to doubt.

Jiang *et al.*[58] reported the bottom-up synthesis of graphene films at low temperature (220~250 ℃) via a radical reaction. Hexabromobenzene (HBB) radicals produced by cleavage of C-Br bonds coupled efficiently on Cu (111) to form graphene films. The charge carrier mobility of as-synthesized graphene evaluated by field effect transistor was 1000~4200 $cm^2\ V^{-1}\ s^{-1}$. The bottom-up synthesis of graphene film via radical coupling reaction is a newly-arisen method, and the quality of as-synthesized graphene film regarding conductivity, thickness uniformity, graphene domain size are not clear.

1.3 Graphene Derivatives - Fluorinated Graphene

Recently there are growing research interests in exploring graphene derivatives. In addition to graphene oxide which is a nonstoichiometric graphene derivative with mainly hydroxyl and epoxide groups randomly distributed on the carbon plane, researchers are interested in stoichiometric graphene derivatives which can be viewed as new two-dimensional crystals. Such stoichiometric graphene derivatives are expected to possess

different electronic properties and may be used as precursors for further chemical modifications of graphene. Furthermore, researchers are interested in opening the band gap of graphene for electronics by exploring graphene derivatives.

Elias *et al.* synthesized graph**ane** (hydrogenated graph**ene**) by reacting graphene with atomic hydrogen in a plasma.[59] Hydrogenation (attaching atomic hydrogen to each of the carbon atoms in graphene) changed the hybridization way of carbon from sp^2 to sp^3, which removed the conducting π-bonds and opened the band gap. Their experimental results showed that single layer graphene exhibited standard ambipolar field effect with charge carrier mobility of ~14,000 $cm^2\ V^{-1}\ s^{-1}$ at room temperature and the half integer quantum Hall effect at cryogenic temperature, while graph**ane** was insulating with charge carrier mobility decreasing to ~10 $cm^2\ V^{-1}\ s^{-1}$ at liquid-helium temperature and did not exhibit the half integer QHE at cryogenic temperature. Graph**ane** was stable at room temperature and could be changed back to graphene by annealing in argon at 450 ℃ indicating that the hydrogenation process is reversible.

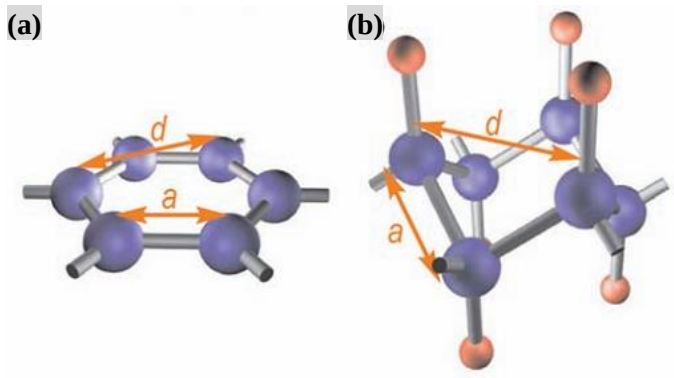

Fig. 14 Schematic showing the crystal structures of (a) graphene and (b) graph**ane**. Carbon atoms are blue spheres and hydrogen atoms are red spheres. (Adapted with permission from ref. 59. © 2009 AAAS.)

Schematic of the crystal structures of graphene and graph**ane** are shown in Fig. 14. Graphene possesses a planar structure with a C-C bond length of 0.142 nm while graph**ane** possesses a chair-like structure with a longer C-C bond length of 0.153 nm due to the change in the hybridization of carbon.

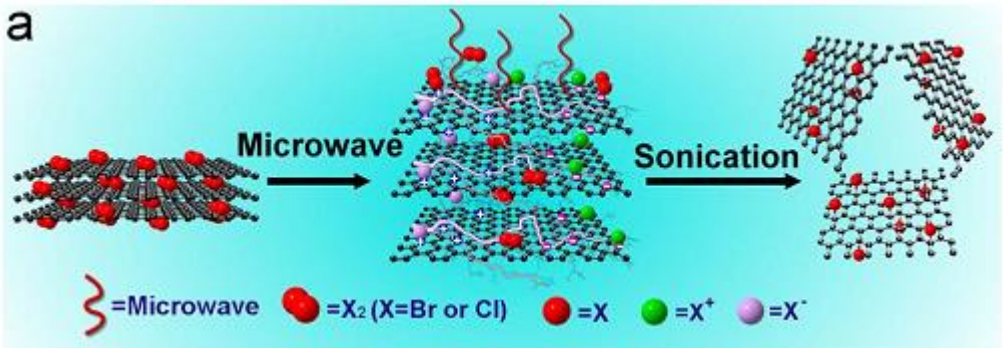

Fig. 15 Schematic for the syntheses of graphene halides (G-Br and G-Cl) using microwave-sparks-assisted halogenation reactions. (Adapted with permission from ref. 60. © 2012 Nature Publishing Group.)

Besides hydrogenated graphene, covalently attaching halogen atoms (F, Cl, Br, I) to the carbon plane have also aroused intense research interests. Zheng *et al.*[60] synthesized chlorine and bromine modified graphite using microwave-sparks-assisted halogenation reactions, and obtained monolayer graphene halide by sonication of the resulting chlorinated or brominated graphite dimethylformamide (DMF). A schematic for the syntheses of graphene halides is shown in Fig. 15. The chlorinated graphene (or graphene chloride) had 21 at% chlorine while brominated graphene had 4 at% bromine. They also synthesized laurylamine modified graphene by using the substitution reaction between a graphene halide (Cl or Br) and laurylamine, which implied that graphene halides are suitable precursors for performing such chemical functionalization of graphene.[60]

Fluorination of graphitic materials has a long history. Graphite fluoride was first reported in the 1930s.[61] Graphite fluoride is mainly used as solid lubricant.[62] The compositions of graphite fluoride can be varied from $(C_2F)_n$ to $(CF)_n$ depending on the reaction conditions.[63] $(CF)_n$ represents the formula of graphite fluoride with saturate fluorine content in which each carbon atom is bonded with a fluorine atom. With the advent of graphene, researchers are interested in synthesizing fluorinated graphene (FG) and exploring its applications in such areas as electronics, optics, and so on. Robinson *et al.*[64] obtained a partially fluorinated graphene film of C_4F composition (i.e. 25 at% fluorine) by fluorination on one side of the CVD-grown graphene film with XeF_2 gas. The as-prepared C_4F film is optically transparent with a calculated band gap of 2.93 eV. They also showed that the same fluorination method could be used to fluorinate both sides of the graphene film to form perfluorographene (CF) which had a calculated band gap of 3.07 eV.

Nair *et al.*[65] synthesized stoichiometric fluorographene or fluorinated graphene (FG) in which each carbon atom is attached by a fluorine atom by exposing graphene crystals (obtained by scotch tape method) to XeF_2. As a two-dimensional (2D) material in the family of fluorinated carbon materials, FG is markedly different from other members including Teflon which is a fluorinated carbon chain (1D) and graphite fluoride (3D). They showed that FG was a high-quality insulator with resistivity $>10^{12}\,\Omega$ and had an optical gap of 3 eV. FG inherited the excellent mechanical strength of its parent graphene with a Young's modulus of 100 N m^{-1} (0.3 TPa, 3 times less than graphene) and sustaining strains of 15%. FG was chemically inert and stable up to 400 ℃ in air, which was similar to Teflon. FG could be

potentially used as an atomically thin insulator or a tunnel barrier in graphene-based devices.[65]

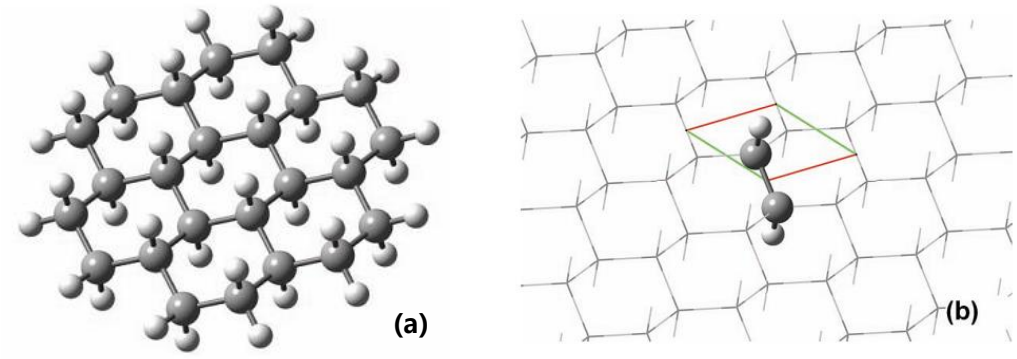

Fig. 16 Models showing the chair-like structure of FG. (a) Ball-and-stick model of FG, big dark grey balls represent carbon atoms and small light grey balls represent fluorine atoms. (b) 2D unit cell (C_2F_2) and translation vectors. (Adapted with permission from ref. 66. © 2010 Wiley.)

Models for the structure of FG are shown in Fig. 16. The structure of FG is similar to that of graph**ane**. The hybridization way of carbon changes from sp^2 in graphene to sp^3 in FG, which leads to the change from planar structure in graphene to chair-like structure in FG. Zboril *et al.* reported that quantum-mechanical calculations revealed that FG was the most thermodynamically stable among five hypothetical graphene derivatives: graph**ane**, fluorinated graphene, chlorinated graphene, brominated graphene and iodinated graphene.[66]

Recently, Wang *et al.*[67] demonstrated that FG could be used to enhance adhesion and proliferation of mesenchymal stem cells (MSCs), and that FG exhibited a neuro-inductive effect via spontaneous cell polarization. They also showed that large-scale produced and patterned FG sheets might be a viable platform for tissue-engineering applications.

1.4 Diethylaminosulfur Trifluoride (DAST) as a Useful Fluorinating Reagent for hydroxyl, Carbonyl/Ketone and Carboxylic Groups

Currently fluorination of carbon materials is mainly performed by exposing them to XeF_2 gas, F_2 gas or F-based plasma. However, XeF_2 is air-sensitive, fluorination with XeF_2 needs to be performed in a glove box; F_2 gas is very reactive and dangerous, fluorination with F_2 requires special equipment and great care; the use of F-based plasma is also not very facile. Since graphene oxide can be synthesized cost-effectively and has many oxygen-containing functionalities in its structure, converting these functionalities to C-F bonds (deoxyfluorination) through methods used in organic chemistry could be a viable way to synthesize fluorinated graphene. With this idea in mind, I did a thorough literature research and found diethylaminosulfur trifluoride (DAST) might be a suitable reagent for such purposes.

Sulfur tetrafluoride (SF_4) was reported to be a useful fluorinating reagent for replacing oxygen with fluorine in hydroxyl, carbonyl/ketone and carboxylic groups.[68] However, SF_4 is gaseous, toxic and corrosive making it hard to handle in organic synthesis. Middleton[69] first reported that aminosulfur fluorides synthesized by substitution(s) of one or two of the fluorine atoms in SF_4 with dialkylamino groups were also useful fluorinating reagents. Aminosulfur fluorides are liquid and thus easier to handle than gaseous SF_4. Middleton showed that diethylaminosulfur trifluoride (DAST) could convert R-C-OH and R-C=O to R-CF, R-CF_2, respectively, with high yields of ~70-90%.[69-70] The chemical structure of DAST is shown in Fig. 17. Lal *et al.*[71] reported that bis(2-methoxyethyl)aminosulfur trifluoride (BAST), a fluorinating reagent similar to DAST, could convert R-COOH to R-CF_3 by two steps, converting R-COOH to R-COF first, then converting R-COF to R-CF_3. The yields for both steps were >90%.

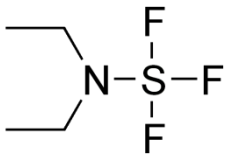

Fig. 17 Chemical structure of DAST.

Since graphene oxide has many hydroxyl groups, minor carbonyl and carboxylic groups, DAST may be a useful reagent for replacing them with fluorine to synthesize fluorinated graphene.

Chapter 2 - Research Objectives, Synthetic Methods and Characterization Tools

2.1 Research Objectives

①Synthesis and characterization of graphene oxide. ②Fluorination of graphene oxide using DAST to synthesize fluorinated graphene. ③Exploring the biological application of graphene oxide

2.2 Synthetic Methods

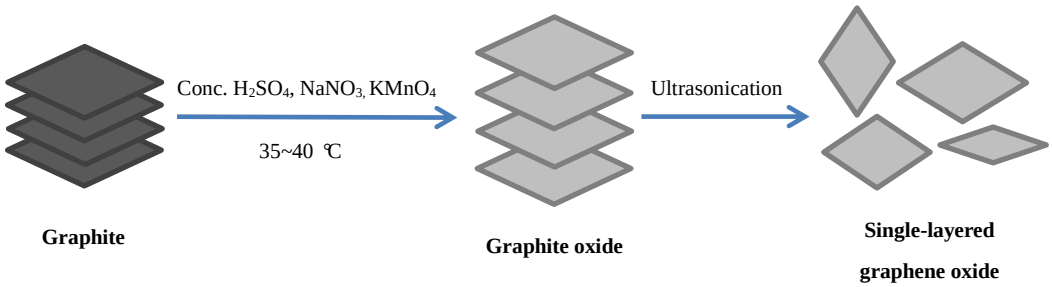

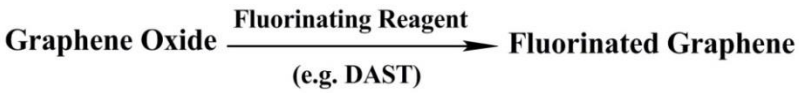

2.3 Characterization Tools

2.3.1 Fourier Transform Infrared Spectroscopy (FTIR)

FTIR stands for Fourier Transform InfraRed spectroscopy, an advanced method of infrared spectroscopy which uses the mathematical process-Fourier transform to convert raw data to actual spectrum. Infrared spectroscopy is a technique which utilizes the interactions of

infrared light with matter to identify unknown materials. Infrared light can be divided into near-infrared (13000-4000 cm^{-1}), mid-infrared (4000-400 cm^{-1}) and far-infrared (400-10 cm^{-1}). The mid-infrared region is the most commonly used because the vibrational excitations of most organic functional groups (e.g. $-CH_3$, -C=C-, O-C=O) and inorganic ions (e.g. CO_3^{2-}, SO_4^{2-}, MnO_4^-) are induced by mid-infrared light.[72]

Infrared light imposed on a molecule does not contain enough energy to cause electronic transitions, but can cause vibrational and rotational changes of the molecule. Possible vibrational rotational motions of a molecule can be categorized into symmetric/asymmetric stretching, scissoring (symmetric in-plane bending), rocking (asymmetric in-plane bending), wagging (out of plane bending) and twisting (out of plane bending). The vibration frequency of a molecule excited by infrared light can be expressed in equation 1.

$$\nu = \frac{1}{2\pi}\sqrt{\frac{k}{(\frac{m_1 m_2}{m_1+m_2})}} \qquad \textbf{Equation 1}$$

, where v is the frequency in cm^{-1}, k represents the force constant in N cm^{-1}, m_1 and m_2 are the masses of two atoms, respectively.[72]

By passing infrared light through a sample and measuring the transmittance or absorbance at each frequency of light, an infrared spectrum is obtained with peaks corresponding to the vibrational frequencies of functional groups in the sample. The vibrational characteristics of functional groups are unique. Therefore, functional groups in the sample can be identified by analyzing the positions and shapes of the peaks in the infrared spectrum.

Since graphene oxide has many oxygen-functional groups and chemical modification can lead to structural changes in these functionalities, FTIR will be a useful technique in analyzing the structure of graphene oxide and structural evolutions resulted by modifications.

2.3.2 Raman Spectroscopy

The main spectroscopies which deal with molecular vibrations are based on processes of infrared absorption and Raman scattering. They are widely used to provide valuable information on the chemical structures of substances by analyzing their characteristic spectral patterns. The phenomenon of inelastic scattering was first observed experimentally in 1928 by Raman and Krishnan. Since then this phenomenon has been referred to as Raman scattering and Raman spectroscopy has been developed.

In infrared spectroscopy, an infrared beam covering a range of frequencies (typically 400~4,000 cm^{-1}) is directed onto the sample, and absorption occurs when the frequency of incident radiation matches that of a molecular vibration. By contrast, in Raman spectroscopy, a single frequency of radiation (typically 514 nm or 633 nm or 785 nm) is employed and the radiation scattered from the molecule is detected. Intense Raman scattering occurs when vibrations cause changes in the polarizability of the electron cloud around the molecule, while intense infrared absorption occurs when vibrations cause changes in the dipole moment of the molecule. Therefore, Raman and infrared spectroscopy are complementary and often used together to give a better view of the molecular structure.[73]

2.3.3 Ultraviolet-Visible Spectroscopy (UV-Vis)

Color is an important feature of matter. For example, polytetrafluoroethylene is white, conjugated graphitic materials (e.g. graphite, carbon nanotubes) are black, transition metals (e.g. Ir, Os) organometallic complexes have various colors depending on the structures of ligands. Human eyes act as spectrometers in analyzing the light reflected from the surface of a solid or passing through a liquid when differentiating matter by color. Sunlight or white light is actually composed of a broad range of radiations in the ultraviolet, visible and infrared regions of the electromagnetic spectrum. When white light passes through or is reflected by a colored substance, a portion of the light is absorbed by the substance and the color of the substance perceived by human eyes is determined by the remaining light which is complementary to the absorbed light. For example, a substance appears yellow if it absorbs indigo light from 420 to 430 nm, while a substance appears red if it absorbs green light from 500 to 520 nm.[74]

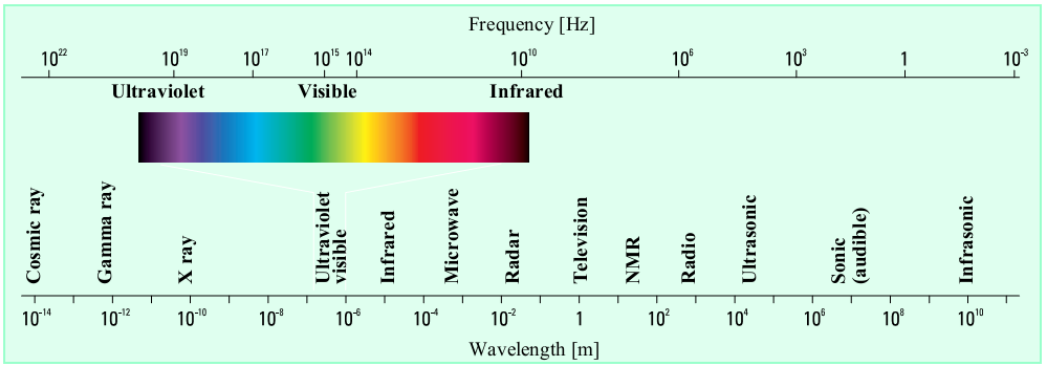

Fig. 18 The electromagnetic spectrum.[75]

The electromagnetic spectrum (Fig. 18) is very broad ranging from short wavelengths (including cosmic ray, gamma ray) to long wavelengths (including sonic, infrared sonic). The ultraviolet (ca. 10-400 nm) and visible radiations (ca. 400 nm-800 nm) constitute only a small

portion of it. However, ultraviolet radiations less than 200 nm are difficult to handle and seldom used for structural analysis of matters. The energies of UV-Vis light range from 1.55 eV to 6.20 eV corresponding to wavelengths of 800 nm and 200 nm, respectively. Such energies are sufficient to cause electronic transitions from low energy orbitals to high energy orbitals in molecules. When the energy of light matches the gap between two energy levels, the light is absorbed and electronic transition or promotion occurs. By passing UV-Vis light through a liquid and detecting the intensity differences between transmitted light and incident light, a UV-Vis spectrometer can determine the wavelengths at which absorption maxima occurs which can be used to identify certain chromophores and conduct quantitative analysis of the amount of molecules based on the Beer-Lambert law.

Under UV-Vis irradiation, $\pi \rightarrow \pi^*$ transition in –C=C- bond and $n \rightarrow \pi^*$ transition in C=O bond can take place. Since graphene oxide contains many such bonds, UV-Vis spectroscopy will be useful in monitoring the structural changes during chemical reduction or modification.

2.3.4 Atomic Force Microscopy (AFM)

Atomic force microscopy (AFM) belongs to the big family of scanning probe microscopies (SPMs). AFM was first described in the literature in 1986. It was created as a supplement to scanning tunneling microscopy (STM) which can only image conductive samples in vacuum. AFM can image samples with high resolution regardless of their conductivities under ambient conditions. The first AFM instrument became available by the early 1990s.

In AFM, a very sharp stylus probe is used to interact with the surface of interest, probing the repulsive and attractive forces between the probe and the surface to give high-resolution topographic imaging of the surface. AFM can be used in contact and non-contact (tapping) mode depending on the properties of the samples and the information to be exacted from it. In the former, the probe is in constant contact with the sample, while in the latter, the probe (or cantilever) is oscillating. AFM is able to image samples in air or fluid environment rather in high vacuum, rendering it particularly useful in imaging polymeric or biological samples in their native states.[76]

AFM is very useful in imaging nano- and micro-sized graphene oxide sheets, providing valuable information on sizes, shapes and thicknesses of graphene oxide sheets.

2.3.5 Scanning Electron Microscopy (SEM)

Scanning electron microscopy is a type of electron microscopy that images samples by scanning it with a focused beam of electrons. The sample's surface topography and composition are attained by collecting various signals produced by interactions between the electron beam and atoms of the sample. The first scanning electron microscope was invented by M. Ardenne in 1937, and the first commercial SEM instrument was developed in 1965 by Cambridge Scientific Instrument Company.

The most common and important imaging mode of SEM is by detecting secondary electrons emitted from the k-shell of the specimen atoms by inelastic scattering interactions with beam electrons. Other imaging modes include backscattered electrons, specimen current, transmitted electrons, electron-beam-induced current, cathodoluminescence, acoustic

thermal-wave microscopy, environmental electron microscopy and imaging with X-rays. The resolution of SEM is somewhere between 1 nm and 20 nm. SEM can image both conductive and non-conductive samples. For imaging non-conductive samples with conventional SEM, coating with conductive materials (e.g. gold, chromium) is required for getting better images. However, environmental SEM can directly image non-conductive samples and wet samples, making it particularly useful in biological applications.[77]

2.3.6 X-ray Photoelectron Spectroscopy (XPS)

X-ray photoelectron spectroscopy, also known as electron spectroscopy for chemical analysis (ESCA), is a powerful surface chemical analysis technique which provides such information as the elemental composition of the surface (top 1~10 nm), empirical formula of pure materials, chemical bonding states of the element in the surface, line-profiling (mapping) and depth-profiling of chemical composition uniformity. The first commercial monochromatic XPS instrument came into being in 1969.

Qualitative XPS (element identification) is based on equation 2, where E_b is the binding energy of a core electron with reference to the Fermi level, E_F, $h\nu$ is the energy of the X-ray being used, E_{kin} is the kinetic energy of the electron, Φ_A is the work function of the analyzer. The energy of the X-ray is known and the analyzer work function is constant, the kinetic energy determines the binding energy and vice versa. Each element has a unique set of XPS peaks at characteristic binding energies, which provides direct identification of them.[78]

$$E_b = h\nu - E_{kin} - \Phi_A \qquad \textbf{Equation 2}$$

An XPS spectrum is usually given by intensity (counts per second) as a function of the binding energy. Besides photoelectron core level and valence band peaks, XPS spectra contain Auger electron peaks, and may also contain satellite peaks and energy loss peaks. Chemical composition analysis (quantification) can be carried out using the low-resolution XPS survey spectra with equation 3, where X_i is the molar fraction of element i, I_i or I_j is the intensity or area of the XPS peak of element i or j, *Si* or *Sj* is the relative sensitivity factor (RSF) of element i or j. In brief, to get the atomic percentage of element i, its XPS signal is divided by its RSF and normalized over all of the elements detected.[78]

$$X_i = \frac{\frac{I_i}{S_i}}{\sum_{j=1}^{n} (\frac{I_j}{S_j})} \qquad \textbf{Equation 3}$$

Chemical bonding states of an element (e.g. C-C, C=C, C-OH, O=C-O) can be obtained from its high resolution XPS core-level spectrum. However, XPS can detect all other elements except for hydrogen (atomic number Z=1) and helium (Z=2). The binding energies of H and He are so small compared with the energy of X-ray thus making the absorption efficiency very small. Ultraviolet photoelectron spectroscopy (UPS) is designed for detecting H and He.

Chemical composition and chemical bonding states analyses are very important to the research of chemical modification and reduction of graphene oxide, therefore XPS is an indispensable tool.

2.3.7 Four-Probe Method for Measuring Thin Film Conductivity

Four-probe method, also called Kelvin method, is a technique that measures resistance using separate pairs of current-carrying and voltage-sensing probes to make more accurate

measurements than traditional two-probe method. In a sheet resistance measurement, several resistances need to be considered as shown in Fig. 19a. The probe itself has a probe resistance *Rp*. A probe contact resistance *Rcp* exists in the interface between the probe tip and the thin film. A spreading resistance *Rsp* arises when the current flows from the probe tip into the thin film and spreads out in the thin film. And the thin film to be measured has a sheet resistance *Rs*. Schematic and equivalent circuit of the four-probe technique are shown in Fig. 19b and Fig. 19c, respectively.

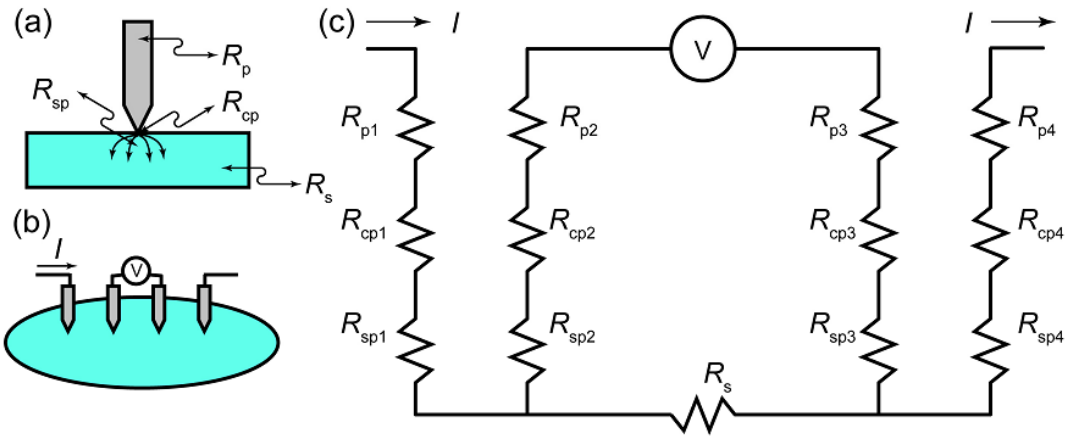

Fig. 19 Measurement of thin film sheet resistance by a four-probe method. (Adapted with permission from ref. 79. © 2011 InTech.)

Two outer probes carry the current and two inner probes sense the voltage. Since the voltage is measured with a high impedance voltmeter, voltage drops across the parasitic resistances (*Rp*, *Rcp*, *Rsp*) of the two inner probes are significantly small and can be neglected. The thin film sheet resistance can be calculated via equation 4:

$$R_s = F_1 \cdot F_2 \cdot F_3 \cdot \frac{V}{I} \qquad \textbf{Equation 4}$$

, where *Rs* is the sheet resistance, *V* is the voltage between the two inner probes, *I* is the current, F_1, F_2 and F_3 are correction factors for collinear probes with equal inter-probe

spacing. F_1 corrects for finite sample thickness, F_2 corrects for finite lateral sample dimensions, and F_3 corrects for placement of the probes with finite distances from the sample edges. For very thin samples (the thickness is less than half of the inter-probe spacing) with the probes being far from the sample edges, F_2 and F_3 are approximately equal to 1.0, and the equation can be simplified as:

$$R_s = \frac{\pi}{ln\,2} \cdot \frac{V}{I} \qquad \textbf{Equation 5}$$

The thickness of the thin film can be determined using SEM. Then its bulk conductivity can be calculated.[79,80]

The four-probe method can eliminate the measurement errors caused by probe resistance, contact resistance and spreading resistance. Therefore it is more accurate than the two-probe method. Conductivity measurement is vital to revealing the quality of reduced graphene oxide. The four-probe method for measuring thin film conductivity will be very useful for the research of chemical reduction of graphene oxide.

Chapter 3 - Synthesis, Characterization of Graphene Oxide and Preparation of Free-Standing Graphene Oixde Thin Films

3.1 Hummers Method and Modified Hummers Method for Graphene Oxide Synthesis

3.1.1 Reaction Mechanisms - Formation of Graphite Intercalation Compounds (GICs)

Modified Hummers Method: Kovtyukhova *et al.*[81] first reported the modified Hummers method for graphite oxide synthesis in 1999. Modified Hummers method involves an additional pre-oxidation step compared with Hummers method. In Kovtyukhova's paper, he claimed that this pre-oxidation step was necessary to avoid the formation of incompletely oxidized graphite-core/graphite oxide-shell particles. Modified Hummers method is now widely used for graphite oxide (or graphene oxide) synthesis, yet it is ambiguous regarding the differences in yield, size distribution of graphene oxide sheets, chemical structure and oxidation degree of graphene oxide compared with Hummers method. Typically in modified Hummers method, graphite is pre-oxidized with conc. H_2SO_4, $K_2S_2O_8$ and P_2O_5, then the pre-oxidized graphite is further oxidized following Hummers method.

Hummers method: Hummers method for graphite oxide synthesis was first reported in 1958.[29] After the discovery of graphene in 2004, people gradually noticed graphite oxide can be exfoliated into single-layered graphene oxide simply by ultrasonication in water. Now Hummers method is also widely used for graphene oxide synthesis. Typically in Hummers

method, natural graphite flakes (or powders) is oxidized into graphite oxide with conc. H_2SO_4, $NaNO_3$ and $KMnO_4$ at 35 ℃. Graphite oxide still possesses a laminar structure with an increased interlayer distance of 0.61 nm~1.2 nm compared with graphite which has an interlayer distance of 0.34 nm.[81]

Formation of graphite intercalation compounds (GICs): The first pre-oxidation step in modified Hummers method involves the formation of graphite intercalation compounds (GICs) as was reported by Tour's group.[82] They found that conc. H_2SO_4 does not spontaneously intercalate into graphite, however, in the presence of oxidants (e.g. $KMnO_4$, $K_2S_2O_8$ or $(NH_4)_2S_2O_8$), conc. H_2SO_4 can intercalate into graphite and lead to the formation of graphite intercalation compounds (GICs). By contrast, I found that the intercalation of conc. H_2SO_4 and $K_2S_2O_8$ into graphite to form GIC can be completed in 15-20 minutes with the help of sonication, while the intercalation needs 6-8 h without sonication.[82]

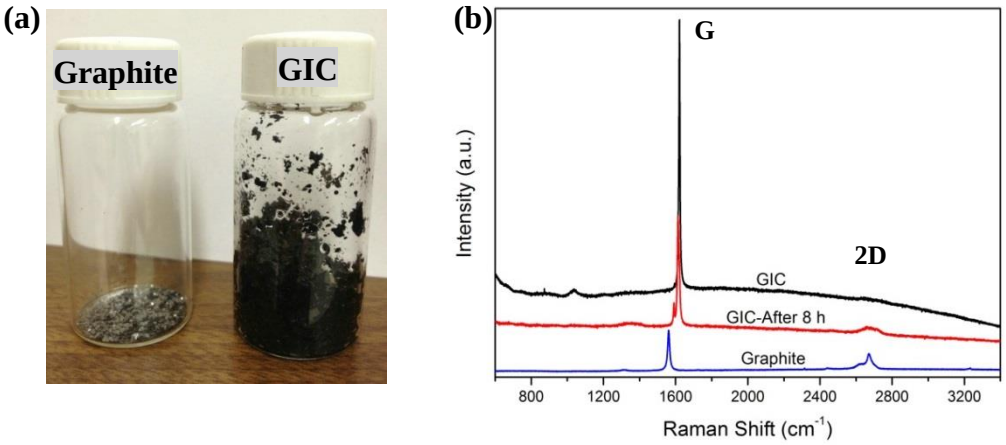

Fig. 20 (a) Photographs and (b) Raman spectra of graphite and H_2SO_4-$K_2S_2O_8$-GIC.

As shown in Fig. 20a, the H_2SO_4-$K_2S_2O_8$-graphite intercalation compound has lost its luster and possesses a much larger volume compared with its parent graphite. The volume expansion is caused by the intercalation of other species (H_2SO_4-$K_2S_2O_8$) into the graphite

lattice which largely increases the inter-layer distance. Raman spectroscopy was further used to characterize the GIC and graphite. Raman measurements were performed with a Horiba Jobin Yvon LabRAM HR 800 Raman spectrometer using a 633 nm excitation laser. The Raman spectrum of graphite (Fig. 20b, bottom) shows two pronounced peaks: G band at ~1580 cm^{-1}, and 2D band at ~2690 cm^{-1}. The Raman spectrum of H_2SO_4-$K_2S_2O_8$-GIC (Fig. 20b, top) shows only one prominent G peak located at 1610 cm^{-1}, which is shifted compared with that of graphite. Another noteworthy aspect is that the intensity of the G band of GIC is a lot higher than that of graphite indicating that intercalation of graphite with other species (or heavy doping) can enhance the G band in the Raman spectrum, which is in accordance with the literature.[2] The Raman spectrum of H_2SO_4-$K_2S_2O_8$-GIC after being exposed to air for 8 h is shown in Fig. 1b, middle. The reappearance of the 2D band indicates the deintercalation of GIC when exposed to air. This can be explained by that concentrated H_2SO_4 from GIC adsorbed water vapors from the air when it is exposed which leads to the deintercalation. Thus the intercalation of concentrated H_2SO_4-$K_2S_2O_8$ with graphite is somewhat reversible.

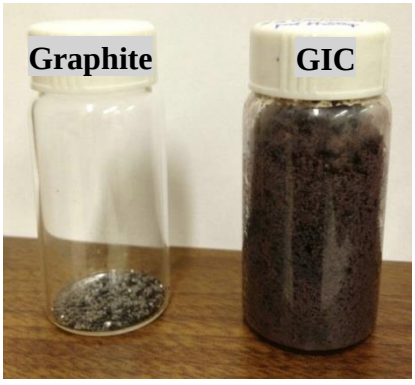

Fig. 21 Photographs of graphite and H_2SO_4-$KMnO_4$-GIC.

Similarly, another concentrated H_2SO_4-$KMnO_4$-GIC (graphite flakes 1.0 g, $KMnO_4$ 3.0 g, concentrated H_2SO_4 10 mL) was prepared with sonication. Again, the intercalation was

accomplished in about 15-20 minutes with the help of sonication, large volume expansion and color change were observed as shown in Fig. 21.

The as-prepared H_2SO_4-$K_2S_2O_8$-GIC and H_2SO_4-$KMnO_4$-GIC may have applications in producing high quality graphene (much less oxidized compared with graphene oxide synthesized by Hummers method) via liquid-phase exfoliation with the help of sonication[55] and MnO_2-graphene hybrid material.[83]

The chemical processes of making graphene oxide in Hummers method involve formation of some kind of H_2SO_4-$KMnO_4$-GIC and meanwhile oxidation on some edges, defects, cracks, and/or vacancies of graphite sheets (carboxylic and carbonyl groups are most likely formed at this stage), further hydrolysis of the GIC affords more oxygen-functional groups attached to the carbon plane (hydroxyl and epoxide groups are most likely formed at this stage). Once the oxygen-containing groups are attached to the graphene plane, the van der Waals forces between graphene planes are minimized, therefore, the exfoliation of graphite (or oxidized graphite) into few-layered graphite or even single-layered graphite (i.e. graphene) is possible by mechanical stirring which is used throughout the whole reaction. Sonication of few-layered graphite oxide leads to mass production of mono-layered graphene oxide.[84-85]

It is worth pointing out that the size of graphite oxide sheet which finally determines the size of graphene oxide sheet is also largely reduced by the hot gas bubbles produced by sonication. Su et al.,[86] Zhou et al.[87] and Zhao et al.[88] reported the synthesis of ultra-large graphene oxide sheets with dimensions of hundreds of micrometers which are much larger than conventional graphene oxide sheets that have lateral sizes in the range of hundreds of nanometers to a few micrometers. In their methods the exfoliation of multi-layered graphite

oxide into single-layered graphene oxide is realized by just mechanical stirring or mild sonication for a short time period of 5 minutes while in conventional method sonication for 30 minutes~1 hour is usually used. Therefore, no sonication or mild sonication should be used in order to get ultra-large graphene oxide sheets with lateral sizes of hundreds of micrometers.

3.1.2 Experimental Procedures - Modified Hummers Method

1. Graphite flakes (3.6 g, Sigma-Aldrich, 100 mesh) were ground with NaCl (30 g) for 20 minutes. Afterwards, copious water was added to dissolve NaCl, the mixture was filtered and washed several times to remove NaCl. The remaining solid was dried at 80 ℃ for 1.5 h.

2. Dry graphite powders (~3.0 g) was added into a solution of $K_2S_2O_8$ (2.5 g), P_2O_5 (2.5 g) and concentrated H_2SO_4 (15 mL, 95-98%). The mixture was kept in an 80 ℃ oil bath for 4 h with stirring. After the dark blue mixture was cooled to room temperature naturally, deionized water was added, followed by filtration and rinsing with copious water. The solid was dried at 60 ℃ for 1.5 h.

3. The pre-oxidized graphite was transferred into a 500 mL round-bottom flask, 69 mL concentrated H_2SO_4 was added. The mixture was stirred for 30 minutes and transferred to a 0 ℃ ice bath. $KMnO_4$ (15 g) was added slowly with stirring to keep the temperature of the mixture below 20 ℃.

4. The mixture was heated for 2 h with stirring in a 35~40 ℃ water bath. Then it was carefully diluted with 140 mL deionized water (violent effervescence occurs with an increase in the temperature to 92~98 ℃) and continued stirring for 30 minutes.

5. Afterwards, the flask was removed from the water bath, and the mixture was transferred to a large beaker. 420 mL deionized water was added, followed by 20 mL 30 wt% H_2O_2 (the color of the suspension turned green). The suspension was stirred for 10 minutes, repeatedly centrifuged at 11,000 rpm for 10 minutes, and washed with 5% HCl for three times, followed by deionized water twice (the precipitate was collected and the supernatant which contained large amounts of salts and small light-weighted particles were thrown away each time).

6. The slurry-like precipitate was re-dispersed in 350 mL Milli-Q water and stirred for 15 minutes. The suspension was treated with bath sonication (operating frequency 33 kHz, power 60 W) for 30 min. Then the suspension was repeatedly centrifuged at 3,000 rpm for 4~5 times to remove any insoluble particles (the supernatant was collected each time).

7. Afterwards the homogenous brown solution was dialyzed against Milli-Q water for 1 week and stored for future use. The concentration was determined by filtering 8.0 mL stock solution using a 0.02 μm Anodisc membrane filter (Whatman), drying the resulting film in a 50 ℃ oven overnight and weighing its mass. The concentration of the solution was about 2.5~3.5 mg/mL using the preparation method described above.

Photographs of as-prepared graphene oxide stock solution and diluted ones are shown in Fig. 22. Graphene oxide solution is homogeneous with no visible particles, and has a dark brown to light yellow color depending on its concentration instead of a black color suggesting that the π-conjugation of graphene has drastically changed after oxidation which leads to different band structures and transitions under visible light excitation. Graphene oxide solution is table for infinite time. The synthesis of graphene oxide by modified Hummers

method is mass production as illustrated by the left photograph in Fig. 22 which shows 250 mL 2.8 mg/mL graphene oxide solution.

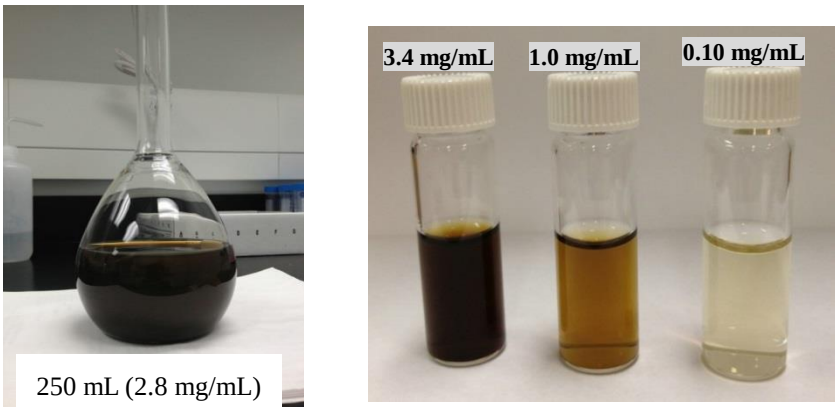

Fig. 22 Photographs showing (left) large-scale synthesis of graphene oxide and (right) graphene oxide aqueous solutions of different concentrations.

3.2 Graphene Oxide Characterization

3.2.1 FTIR Characterization

Graphene oxide solid obtained by vacuum filtration was finely ground with KBr, and then compressed into thin pellets for FTIR characterization. The FTIR spectrum was collected using a Bruker Tensor 37 FTIR spectrometer.

The characteristic features of the FTIR spectrum of graphene oxide (Fig. 23) are the strong and broad band at 3424 cm-1 which can be attributed to the O-H stretching of carboxylic, hydroxyl groups and absorbed water, weak bands at 2928 and 2851 cm^{-1} which can be attributed to the C-H symmetric and asymmetric stretching of CH_2 groups, 1725 cm^{-1} attributed to the C=O stretching of ketone, carboxylic and/or ester groups, sharp and middle strong band at 1628 cm^{-1} attributed to carboxylic groups or the C=C stretching, 1401 cm^{-1} attributed to the O-H bending of carboxylic, hydroxyl groups and absorbed water, 1227 cm^{-1}

attributed to the C-OH stretching of carboxylic and hydroxyl groups, 1057 cm^{-1} attributed to the C-O-C stretching of epoxide and/or ester groups.[34,89-90]

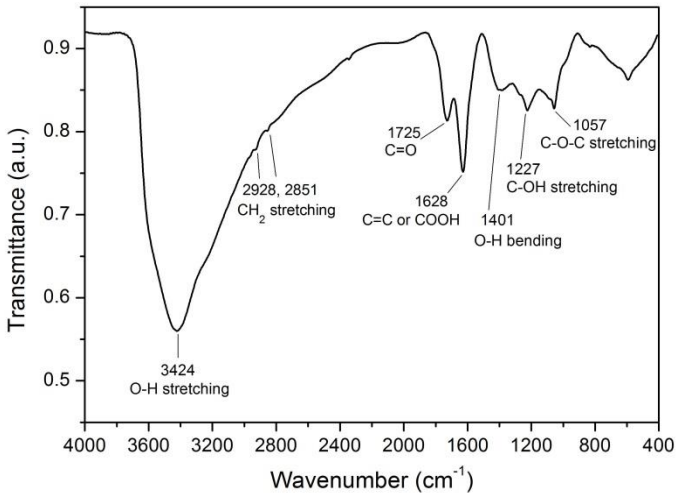

Fig. 23 FTIR spectrum of graphene oxide.

3.2.2 UV-Vis Characterization

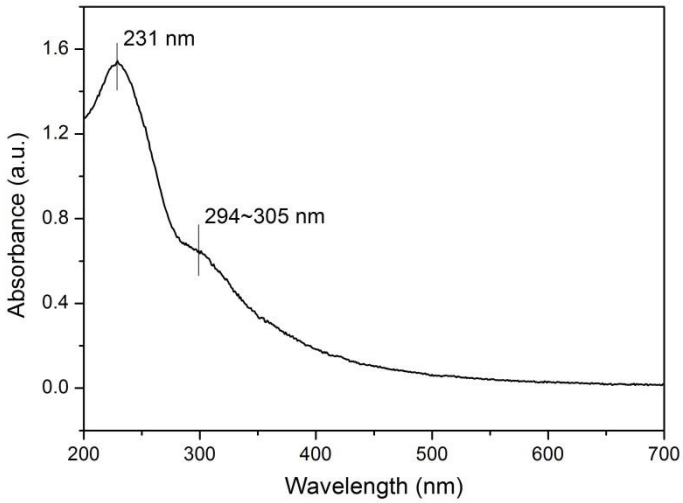

Fig. 24 UV-vis spectrum of graphene oxide.

Diluted graphene oxide aqueous solution was used for UV-vis characterization. The measurement was performed with a Thermo Scientific GENESYS 10S UV-Vis spectrophotometer. The characteristic features in the UV-vis spectrum of graphene oxide (Fig.

24) are the sharp peak at 231 nm which can be attributed to the **π→π*** transitions of -C=C- bonds, the broad and less obvious peak at 294-305 nm which can be attributed to the **n→π*** transitions of -C=O bonds.[91-92]

3.2.3 AFM Characterization

SiO_2/Si substrates were sonicated in deionized water for 15 minutes and blown dry with pure nitrogen gas, followed by the same treatment with acetone. The pre-cleaned substrates were further cleaned by oxygen plasma in a glove box. GO sheets were deposited on the pre-treated SiO_2/Si substrates by spin-coating of a GO H_2O-EtOH dispersion (volume ratio of H_2O to EtOH is 1:9) at 3,000 rpm. As the volatile solvent evaporated away quickly, GO sheets stuck to the substrates because of van der Waals force. AFM characterization was performed with a Nanoscope MultiMode^{TM} AFM instrument in the taping (non-contacting) mode at a scan rate of 1.0 Hz, and a silicon probe with a resonant frequency of 300 kHz was used. Some typical AFM images are shown in Fig. 25. GO sheets are of irregular shapes with sizes in the range of hundreds of nanometers to a few micrometers.

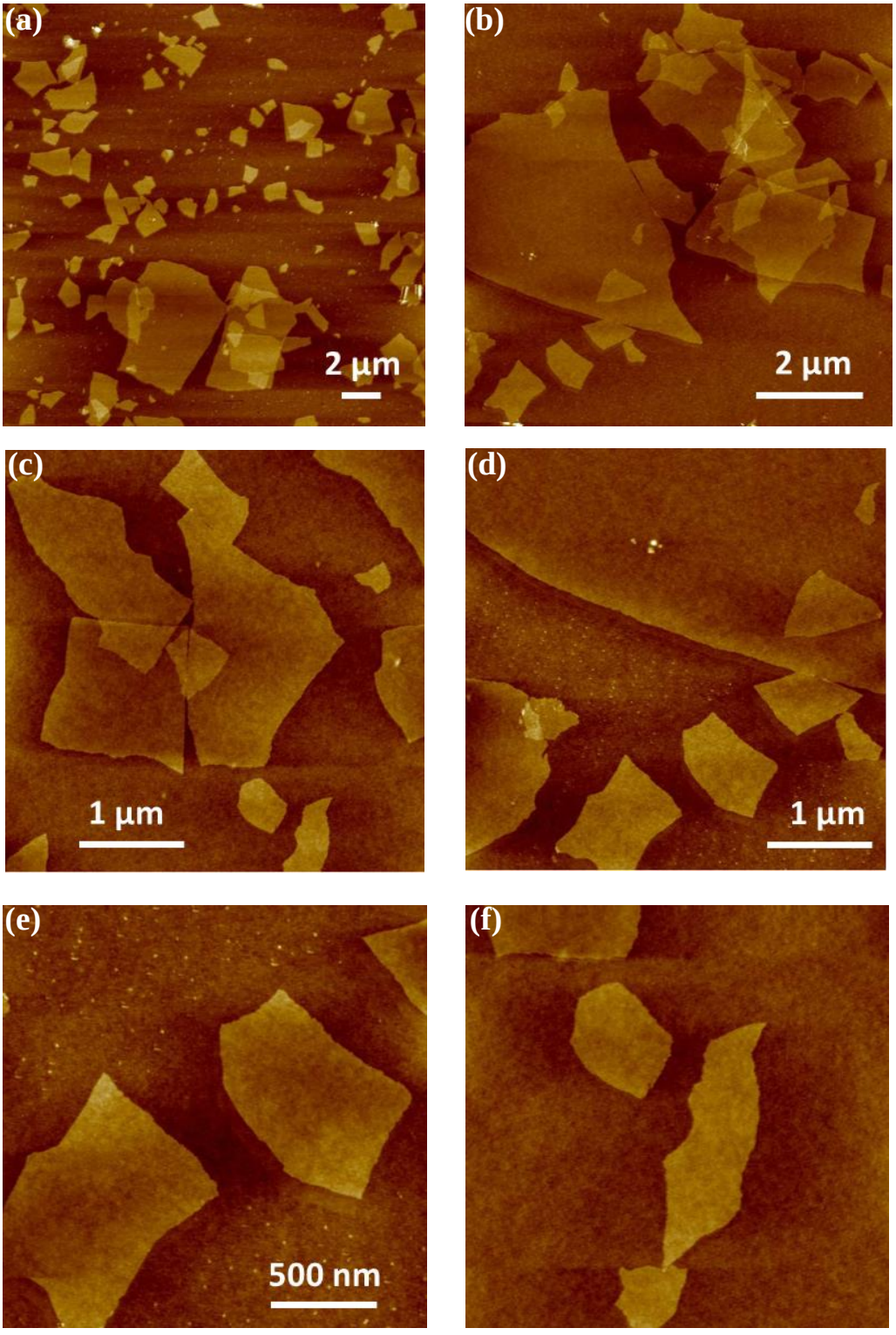

Fig. 25 AFM images showing graphene oxide sheets on SiO_2/Si substrates at different resolutions. Resolutions of the images are as follows: (a) 20 µm × 20 µm, (b) 8 µm × 8 µm, (c) 4 µm × 4 µm, (d) 4 µm × 4 µm, (e) 2 µm × 2 µm, (f) 8 µm × 8 µm.

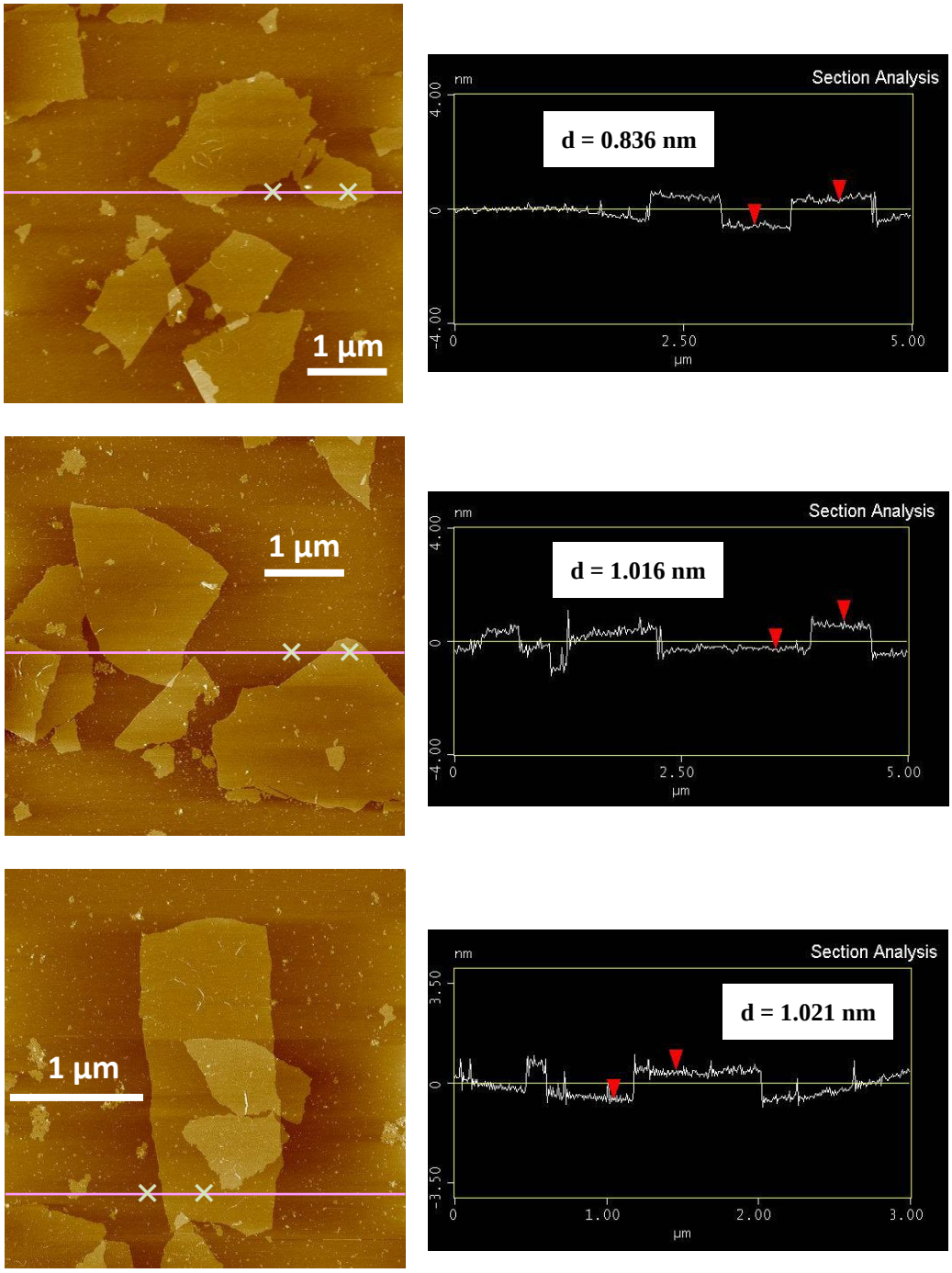

Fig. 26 (Left) AFM images of graphene oxide sheets and (right) height profiles along the pink lines indicated in the AFM images showing the thickness of graphene oxide.

Thickness Analysis:

Height profiles along the pink lines indicated in the AFM images are shown in Fig. 26. The red triangle represents the AFM tip. The height is larger when the red triangle is on the surface of a GO sheet compared with that when the red triangle is on the substrate. The height difference represents the thickness of a GO sheet, which is 0.8~1.1 nm indicating the as-synthesized GO is single-layered according to the literature.[35] Compared with pristine graphene (unoxidized) which has a van der Waals thickness of 0.34 nm, GO is thicker due to the covalently bonded oxygen-containing groups on both sides of the carbon plane.

Phase imaging in tapping mode AFM measures the phase shift or lag of an oscillating cantilever between driving signal and AC output signal. Phase images can also reveal the morphology of the sample. Some typical phase images are shown in Fig. 27 left. These phase images evidently show the sheet-like structure of GO. Although these 2D GO sheets seem rigid on the SiO_2/Si substrates, they might be flexible in solutions as has been suggested by Ruoff and co-workers.[90] 3D topological view images of GO sheets on SiO_2/Si substrates were also obtained (Fig. 27 right). The surfaces of GO sheets are not very flat in these 3D topological images, which might be explained by that the functional groups (hydroxyl and epoxide) on the carbon plane are different which leads to variations in the thicknesses. Another reason might be that the attachment of oxygen-functional groups to the carbon plane substantially changes the hybridization ways of carbon (from sp^2 to sp^3), which destroys the flat structure of conjugate carbon plane.

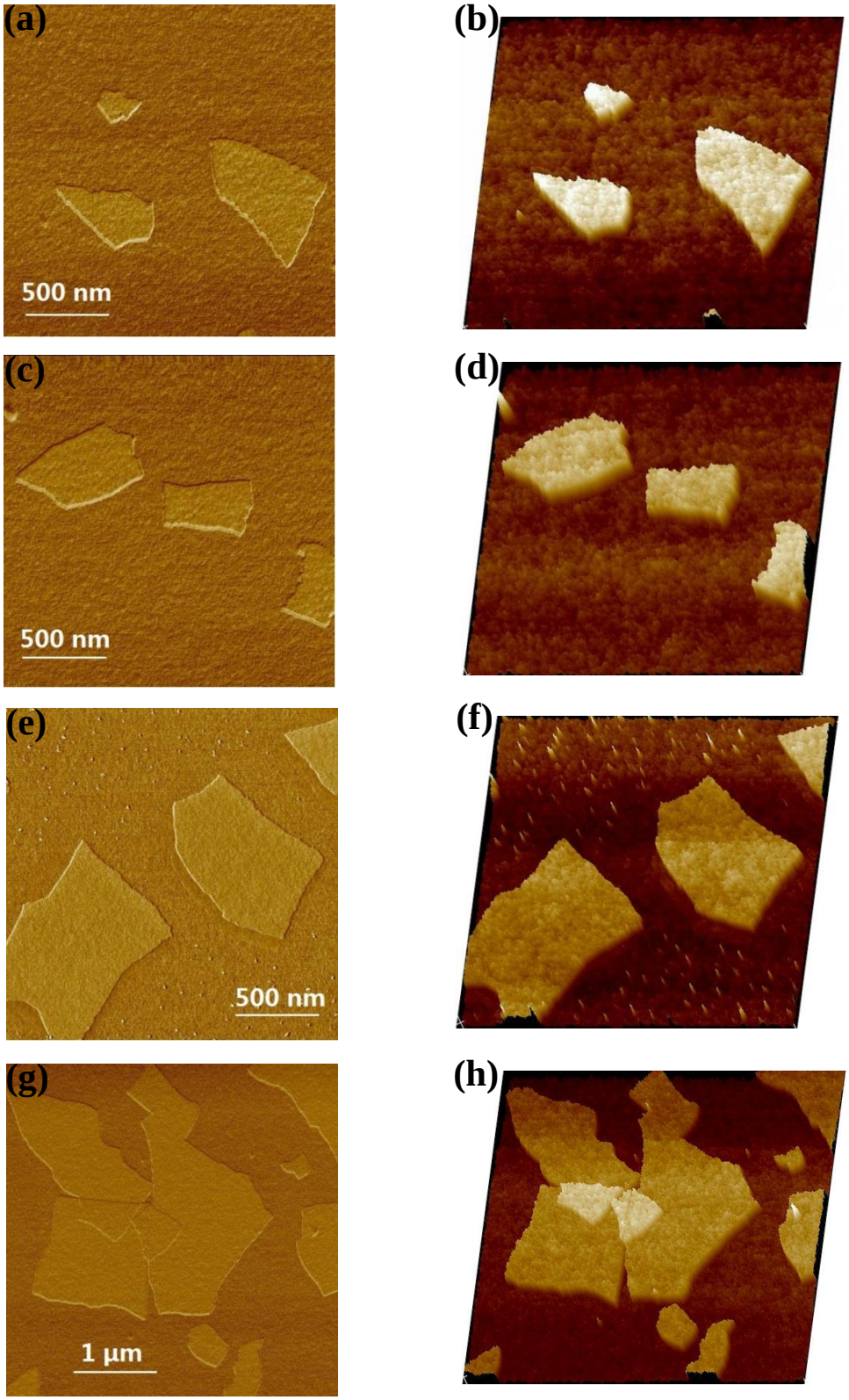

Fig. 27 AFM phase and 3D topographical images of graphene oxide sheets on SiO_2/Si substrates. a, c, e, g are phase images, and b, d, f, h are corresponding 3D topographical images.

3.2.4 Raman Characterization

A small piece of graphene oxide film obtained by vacuum filtration or natural graphite flake (Sigma-Aldrich) was put on a glass slide for Raman Characterization. All Raman measurements were performed with a Horiba Jobin Yvon LabRAM HR 800 Raman spectrometer using a 633 nm excitation laser. A ×50 objective was used.

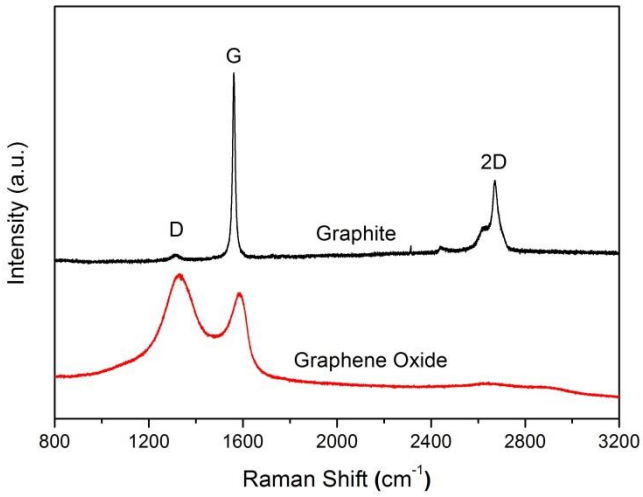

Fig. 28 Raman spectra of graphene oxide and graphite.

In the Raman spectrum of graphite, the small D band at ~1317 cm^{-1} arises from the first order of zone-boundary phonons and is present only in defected graphite. The small D band indicates graphite has few defects. The intensity ratio of D band to G band is widely used to quantify the amount of defects in graphitic materials (graphite, graphene, carbon nanotubes). The strong G band at ~1562 cm^{-1} is due to the doubly generate zone center E_{2g} mode. The 2D band is due to the second order of the zone-boundary phonons and is double of the D band. The 2D band of graphite actually consists of two bands, $2D_1$ of lower intensity at 2625 cm^{-1}, and $2D_2$ of higher intensity at 2674 cm^{-1}. By contrast, the 2D band of graphene is a single sharp peak.[93-94]

The Raman spectrum of GO shows two pronounced peaks, the D band at ~1330 cm^{-1}, and the G band at ~1585 cm^{-1}. The broadening of the D band and G band, and the much higher intensity ratio of D to G than bulk graphite indicates GO has lots of defects. Notably, no 2D band is observed in GO, suggesting the structure of GO is much different from graphene or graphite because of the covalent bonding of considerable amount of oxygen-containing groups.

3.2.5 XPS Characterization

Small pieces of GO solid obtained by vacuum filtration were used for XPS characterization. The XPS measurements were performed with a Thermo Scientific ESCALAB 250Xi XPS spectrometer in Prof. Tong Leung's lab (University of Waterloo). Dual Al-Kα X-ray (1486.6 eV, 150 W) with flood gun (0.2 mA) was used to solve the charging issue since GO is insulating. CasaXPS was used for the deconvolution of XPS peaks.

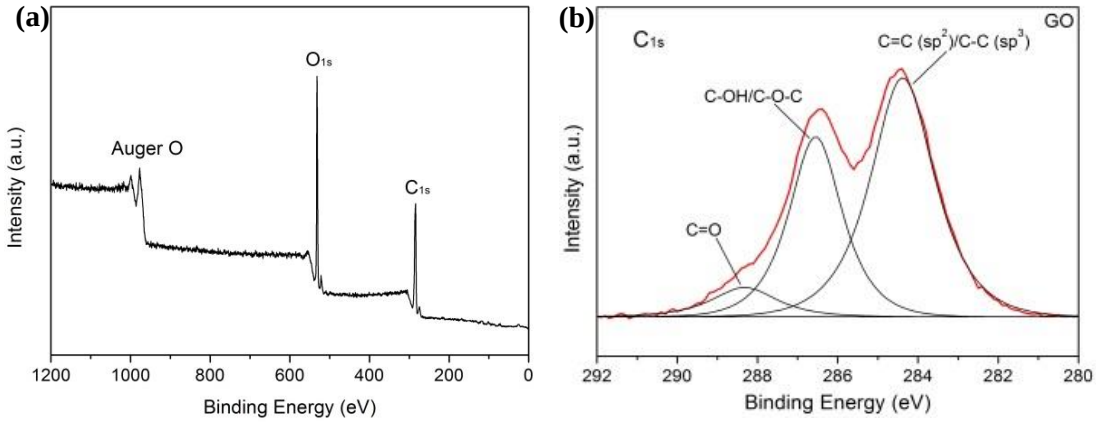

Fig. 29 (a) XPS survey spectrum and (b) C_{1s} spectrum of graphene oxide (red line is the experimental data and black lines are the fitted peaks).

Fig. 29a shows the XPS survey spectrum of as-prepared graphene oxide. Only C (binding energy 284.5 eV) and O (binding energy 532.0 eV) were detected with the absences of other elements such as S and Mn which are common contaminants, suggesting the as-prepared graphene oxide was of high purity. Quantitative analysis based on the XPS survey spectrum showed that the atomic percentages of C and O were 66.01% and 33.99%, respectively. (The relative or atomic sensitivity factors (RSF or ASF) of C and O are 0.296 and 0.711, respectively.) The high resolution C1s spectrum of graphene oxide (Fig. 10b) could be fitted into three main peaks, C=C (sp^2)/C–C (sp^3) at 284.4 eV, C–OH/C–O–C (hydroxyl and epoxide) at 286.6 eV, C=O (carbonyl) at 288.3 eV.[36,91]

3.3 Preparation of Free-Standing Graphene Oxide Thin Films (or Papers)

Free-standing films or papers play an important role in modern technological society. They can be used as protective layers, filter membranes for separation applications, components in batteries or supercapacitors.[95] Graphene oxide, the oxidized form of graphene, is very hydrophilic due to the covalently-bonded oxygen-containing groups, which suggests that graphene oxide is compatible with aqueous-phase processing. Nair et al.[96] reported that submicrometer-thick graphene oxide membranes allow unimpeded permeation of water while they are completely impermeable to liquid, vapors and gases including helium. These graphene oxide membranes were made by spin-coating of graphene oxide aqueous solutions on Cu foils, followed by polymer masking and etching off the underneath copper. Eda et al.[97] reported large-area ultrathin (1~5 layer) films of reduced graphene oxide for transparent and

flexible electronics. In their method, large-area graphene oxide films on filter membranes were first made by vacuum filtration, and then transferred onto plastic substrates, followed by chemical and thermal reduction to recover the conductivity.

While ultrathin graphene oxide films with thicknesses below hundreds of nanometers are important to separation technology, transparent and flexible electronics, macroscopic free-standing graphene oxide films with thicknesses from a few micrometers to tens of micrometers or even higher are expected to find applications in thin film batteries or supercapacitors, biomedical areas, mechanically strong and stiff materials with lamellar structures.[98-101] Currently there are two main methods for making macroscopic free-standing graphene oxide thin films, one is vacuum filtration or flow-directed assembly, the other is self-assembly at the water-air interface.

3.3.1 Vacuum Filtration

Dikin et al.[95] first reported the use of vacuum filtration or flow-directed assembly to prepare free-standing graphene oxide thin film or paper. In a typical experiment, 3.0 mL graphene oxide solution (concentration 0.93 mg/mL) was filtered using an Anodisc membrane filter (diameter 25 mm, pore size 0.02 μm, Whatman), and the film was carefully peeled off the filter using a razor blade.

Fig. 30 shows the digital image of a free-standing graphene oxide film and SEM (Zeiss LEO 1550) image of its cross-section. The film is flexible and mechanically strong enough to be handled with a tweezer. The thickness of the resulting film is about 6.5 μm. The SEM image of the cross-section clearly shows the highly ordered lamellar structure.

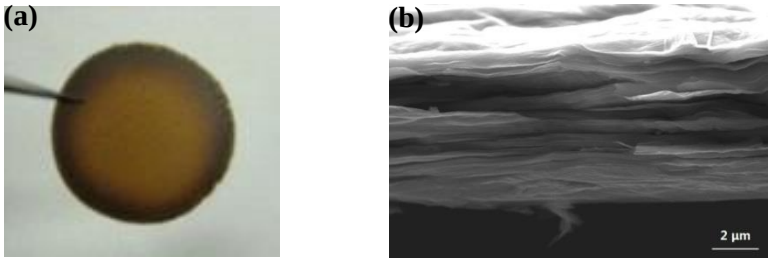

Fig. 30 (a) Photograph of a graphene oxide thin film, and (b) SEM image showing the cross-section of the film

The mechanism of forming thin films with highly ordered lamellar structure lies in that graphene oxide sheets first blocked the pores in the filter membrane, and the sheets come close to each other as the water vaporization on the top of the solution also occurs during the filtration which makes the solution denser and denser, the interactions between sheets are stronger as a result, and the sheets choose to inter-tile with each other. The small amount of water molecules between the sheets can also act as a smoothing component to facilitate the formation of layered structure. Finally, van der Waals forces and hydrogen bonds hold the sheets tightly and mechanically strong graphene oxide thin films with highly ordered lamellar structure are formed as a result.[95]

Ruoff's group reported that the as-prepared graphene oxide papers have excellent mechanical properties with a modulus of ~32 GPa and a tensile strength of ~72.2 MPa, both of which values are higher than carbon nanotube thin films.[95]

3.3.2 Self-Assembly at the Water-Air Interface

Chen et al.[102] first reported the method of efficiently making graphene oxide thin films (typically a few micrometers to tens of micrometers) by self-assembly of graphene oxide

sheets at the water-air interface. This method is more efficient than the vacuum filtration method. This method usually takes 1~2 hours to make the films while the vacuum filtration method usually takes more than 12 hours or even 1~2 days. In a typical experiment, graphene oxide solutions with concentrations from 1.0 mg/mL to 3.0 mg/mL were put in polystyrene weighing dishes. The solutions were heated in an 80~90 ℃ oven for 1~2 hours. Then the weighing dish was taken out and the small amount of solution under the film was carefully poured out. Afterwards the weighing dish was put back into the oven to completely dry the film. After the film is dry, it is easy to peel off the weighing dish since graphene oxide is not sticky to polystyrene materials. A digital image of a free-standing graphene oxide film (diameter 64 mm) prepared in this thesis using this method is shown below.

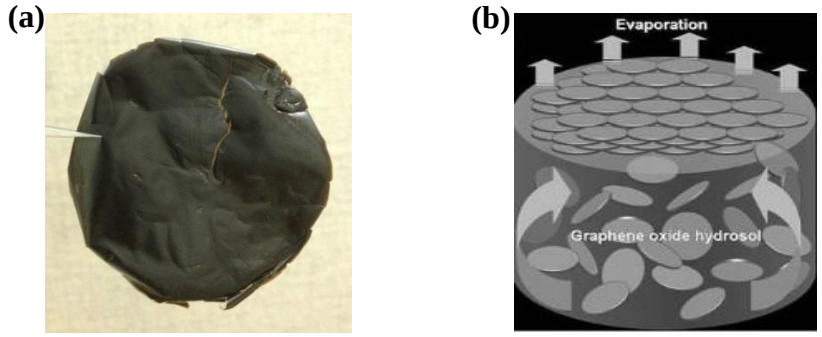

Fig. 31 (a) Digital image of a free-standing graphene oxide film prepared in this thesis by self-assembly at the water-air interface, (b) schematic of the film formation mechanism.[102]

Schematic of the mechanism for this method is shown in Fig. 31b. When a graphene oxide water solution is heated, water vaporizes and lifts up graphene oxide sheets in the solution to the water-air interface. Graphene oxide sheets tend to tile on each other at the interface due to the effect of surface tension. Then van der Waals forces and strong hydrogen bonds hold the sheets tightly. Mechanically strong graphene oxide film is formed as a result.

Besides time-saving, another advantage of this method is that large-area graphene oxide film can be achieved via this method while the area of graphene oxide film is usually limited by the size of filtration apparatus in the vacuum filtration method. However, the mechanical properties of graphene oxide thin films prepared by this method are not as good as those prepared by the vacuum filtration method. The modulus and tensile strength of the former were reported to be ~12.7 GPa, ~67.7 MPa, respectively, both of which are lower than the reported values for the latter (32 GPa, 72.2 MPa, respectively).[102]

3.4 Conclusions and Future Aspects

Graphene oxide, a 2D carbon material decorated with abundant oxygen-containing groups (mainly hydroxyl, epoxide and carboxylic groups), can be massively and cost-effectively produced by Hummers method. Graphene oxide is a lot more hydrophilic than pristine graphene due to the oxygen-functionalities. The concentration of graphene oxide in water is >4 mg/mL. The thickness of graphene oxide is between 0.8 and 1.1 nm. Raman characterization shows that graphene oxide bears many defects in its structure which are created by the severe oxidation during the synthesis process. Graphene oxide sheets produced by Hummers method are of irregular shapes with sizes in the range of hundreds of nanometres to a few micrometres. Free standing and mechanically strong graphene oxide thin films (or papers) can be prepared by vacuum filtration of graphene oxide aqueous solution or self-assembly of graphene oxide sheets at the water-air interface.

Future aspects lie in gaining further insights into the oxidation process in Hummers method and elucidating the chemical structure of graphene oxide. Using solution-based chemical methods to decorate graphene sheets with metal or metal oxide nanoparticles for energy and sensor applications, to prepare graphene-polymer nanocomposites are also future directions.

Chapter 4 – Exploring the fluorination of Grpahene Oxide Using DAST - Chemical Reduction of Graphene Oxide

4.1 Experimental Procedures and Observances

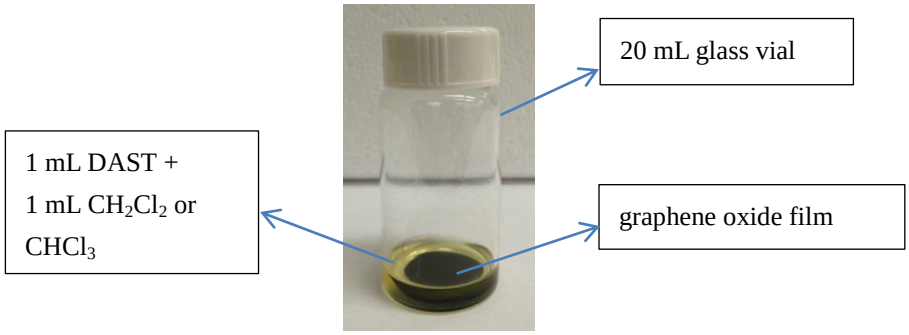

Fig. 32 Schematic of the experimental setup for the reaction of graphene oxide film with DAST.

GO thin films (thickness ~6.5 μm) were put in sealed 20 mL glass vials which contain 1 mL DAST (Matrix Scientific) and 1 mL CH_2Cl_2 or $CHCl_3$ as solvent. Moisture in the vial was not intentionally removed since small amount of HF produced by the reaction of DAST with water could facilitate the fluorination reaction.[71] Another reason was that the amount of DAST added for the reaction was excessive, ruling out the scenario that all the DAST reacted with moisture and rendered the fluorination fail. The vials were kept at 0 ℃, room temperature and 50 ℃, respectively, for reduction and fluorination. For reactions at 0 ℃ and room temperature, CH_2Cl_2 was used as solvent and the reaction time was 1 week. For reaction at 50 ℃, $CHCl_3$ was used as solvent and the reaction time was 17 h. After the reactions were complete, the films were carefully taken out of the vials using a tweezer and soaked in CH_2Cl_2 several times, followed by deionized water to wash away by-products adsorbed on the films. (Direct contact of DAST with water should be avoided in any case since DAST reacts

violently with water!) The films were referred to as reduced graphene oxide-rGO (0 ℃), rGO (R.T.) and rGO (50 ℃), respectively.

Schematic of the experimental setup for the reaction of graphene oxide film with DAST is shown in Fig. 32.

Color Change and Hydrophobicity Change of the Film:

Color change from brownish in GO to black in rGO were observed after DAST treatment (Fig. 33). And rGO (50 ℃) film is more lustrous than the other two rGO films.

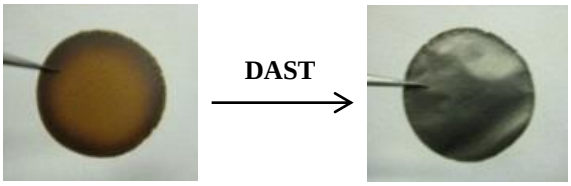

Fig. 33 Digital images of GO and rGO (50 ℃) showing the color change after DAST treatment.

During the washing of rGO films with water, they were observed to be very hydrophobic. A comparison of water contact angle between rGO and GO was conducted to verify this. The digital image (Fig. 34) was taken immediately after one drop of deionized water was placed on each of the films. Obviously rGO (50 ℃) was more hydrophobic than GO.

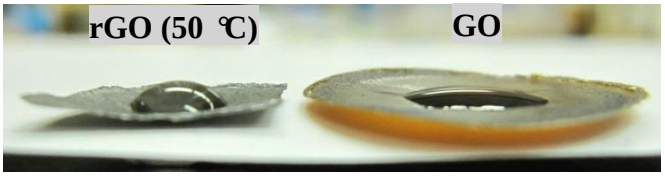

Fig. 34 Water contact angle comparison of rGO (50 ℃) and GO thin films.

4.2 Characterization

4.2.1 XPS Characterization

In order to gain insights into the compositional and structural changes of GO by DAST treatment, XPS characterization was carried out.

Small pieces of rGO films were used for XPS characterization. XPS measurements were performed with a Thermo Scientific ESCALAB 250Xi XPS spectrometer. Monochromatic Al-Kα X-ray (1486.6 eV, 150 W) without flood gun was used.

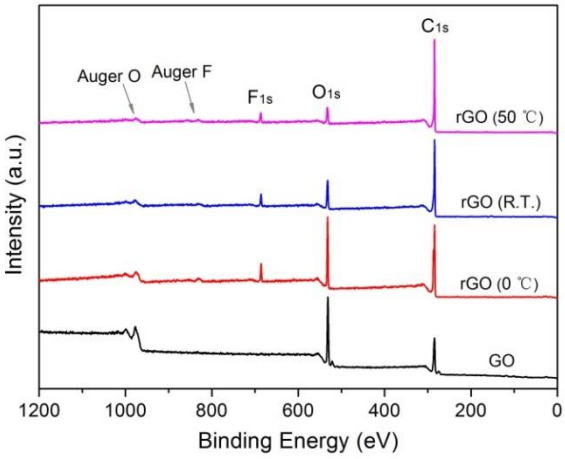

Fig. 35 XPS Survey spectra of graphene oxide film and reduced graphene oxide films.

	C (at%)	O (at%)	F (at%)	C/O
rGO (50 ℃)	86.71	9.73	3.55	8.91
rGO (R.T.)	81.33	15.20	3.47	5.35
rGO (0 ℃)	74.50	21.95	3.54	3.39
GO	66.01	33.99	0	1.94

Table 1 Atomic ratio of GO and rGO determined from XPS survey spectra.

Fig. 35 shows the XPS survey spectra of GO and rGO. Quantitative analysis based on the XPS survey spectra was performed with CasaXPS, the relative sensitivity factors of C, O, F are 0.296, 0.711 and 1.000, respectively. The atomic percentages of GO and rGO are listed in table 1. The fluorine content of all rGO samples is ~3.5 at% and does not change much with reaction temperatures. However, the oxygen content decreases significantly when the reaction temperature is increased from 0 ℃ to 50 ℃. The C/O atomic ratio increases from 1.94 in GO to 5.35 in rGO (R.T.) and 8.91 in rGO (50 ℃). The C/O ratio of 8.91 in rGO (50 ℃) is slightly higher than the sequential $NaBH_4$ and concentrated H_2SO_4 reduced GO (C/O ratio is 8.57)[34] and close to the hydrazine reduced GO (C/O ratio is 10.3)[35], which indicates the effective reduction of GO by DAST.

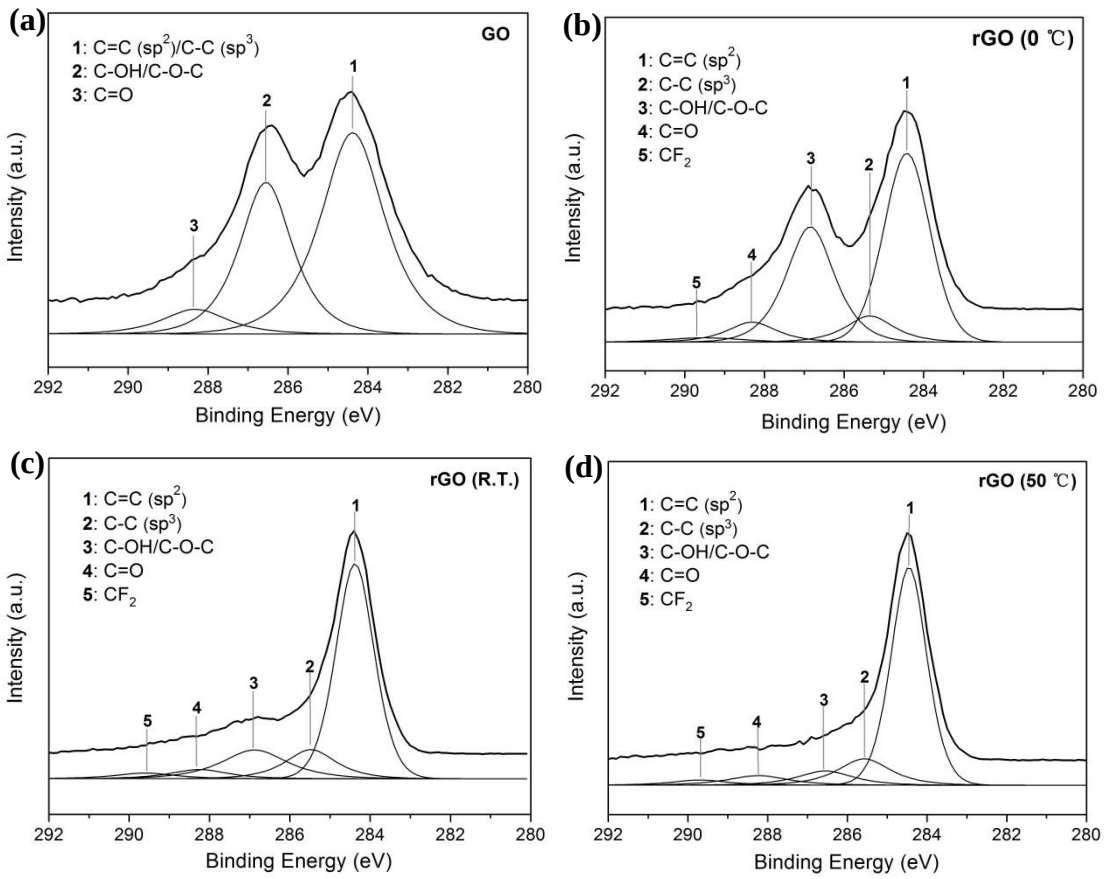

Fig. 36 High resolution XPS C_{1s} spectra of GO and rGO films.

High resolution XPS C_{1s} spectra are further used to confirm the reduction and fluorination. The C_{1s} spectrum of graphene oxide (Fig. 36a) can be fitted into three peaks, C=C (sp^2)/C–C (sp^3) at 284.4 eV, C–OH/C–O–C (hydroxyl and epoxide) at 286.6 eV, C=O (carbonyl) at 288.3 eV.[36,91] By contrast, the C_{1s} spectra of rGO can be fitted into five peaks, C=C (sp^2) at 284.4 eV, C–C (sp^3) at 285.6 eV, C–OH/C–O–C (hydroxyl and epoxide) at 286.6 eV, C=O (carbonyl) at 288.3 eV, and CF_2 at 289.7 eV.[36,103] The C=C (sp^2) peaks of rGO (R.T.) and rGO (50 ℃) are narrower than that of GO. The C–OH/C–O–C and C=O peaks of rGO (50 ℃) decrease significantly compared with GO suggesting effective reduction.

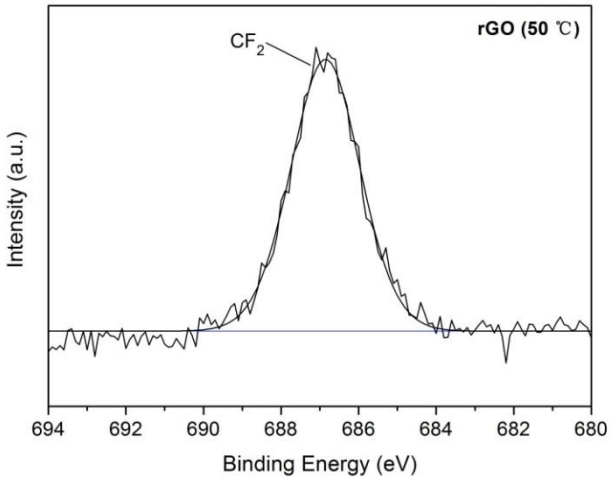

Fig. 37 XPS High resolution F_{1s} spectrum of rGO (50 ℃).

High resolution F_{1s} spectrum of rGO (50 ℃) (Fig. 37) can be fitted into a single peak at 686.9 eV corresponding to covalent C-F bond.[67,103]

However, the middle part of the film is not reacted as justified by the XPS survey spectrum (Fig. 38) on the cross section of rGO (50 ℃) film. XPS characterization on the cross section of the film was done by shining the X-ray on the cross section and collecting resulting data. The chemical composition determined from this survey spectrum is: C 76.22

at%, O 22.54 at%, F 1.23 at%. The O/C ratio of the cross section of the film is 0.30 which is much higher than that of the surface of the film which is 0.11. This lends support to that the middle part of the film is not reacted probably because it cannot be accessed by DAST.

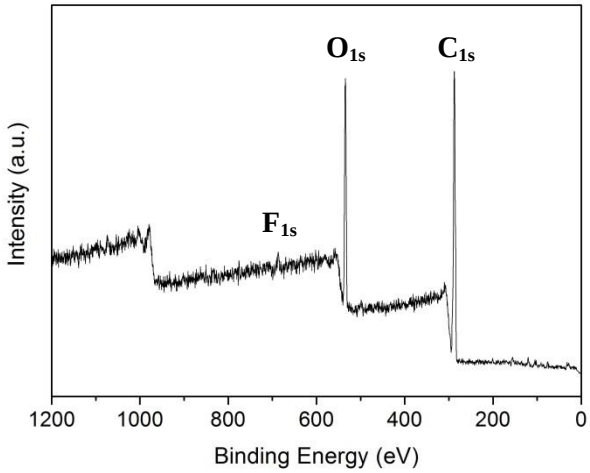

Fig. 38 XPS survey spectrum on the cross-section of rGO (50 ℃) film.

4.2.2 FTIR Characterization

FTIR was used to investigate the chemical changes of GO caused by DAST treatment.

Small pieces of rGO and GO films were finely ground with KBr and pressed into thin pellets for FTIR characterization. The FTIR spectra were collected with a Bruker Tensor 37 FTIR spectrometer.

The FTIR spectra of GO and rGO (50 ℃) are shown in Fig. 39. After the treatment with DAST, the band at 1725 cm^{-1} decreases significantly since most of the C=O groups are converted into CF_2 groups. The new band at 1580 cm^{-1} may be attributed to the stretching vibration of isolated C=C bonds formed by elimination of hydroxyl groups. Another new band at 1200 cm^{-1} can be attributed to the stretching of covalent C-F bond which is well

known for graphite fluoride, fluorinated carbon nanotubes and fluorinated graphene.[63,67,104-105] This band is weak since the fluorination is limited as revealed by XPS characterization. The band at 1100 cm^{-1} is likely due to the stretching of C-O-C group (epoxide) since the reactivity of DAST towards epoxide is low according to the literature.[70,106] Epoxide might account for the residual oxygen in rGO (50 ℃) as well. The overlapping of C-F stretching with C–O–C stretching results in a broad band from 1000 cm^{-1} to 1300 cm^{-1}. The fingerprint region from 1000 to 1750 cm^{-1} of rGO (50 ℃) is less evident than that of GO suggesting reduction of GO. The persistently strong band at 3442 cm^{-1} of rGO (50 ℃) is largely due to the moisture in the KBr pellets.

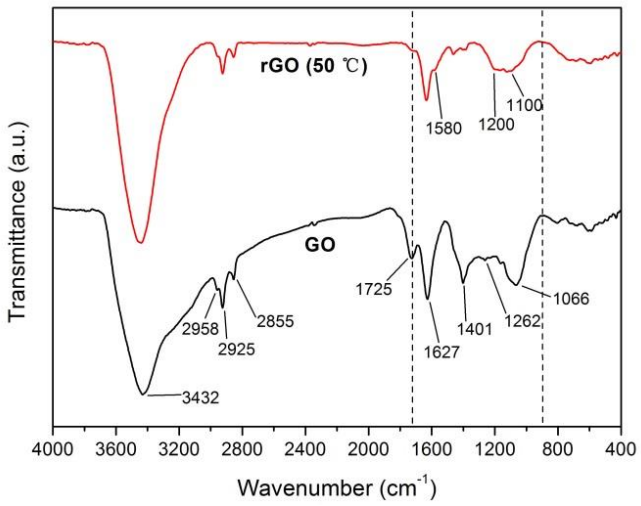

Fig. 39 FTIR spectra of rGO (50 ℃) and GO.

4.2.3 Raman Characterization

Small of pieces of GO and rGO films were placed on glass slides for Raman characterization. All Raman spectra were collected with a Horiba Jobin Yvon LabRAM HR 800 Raman spectrometer using a 633 nm excitation laser and a ×50 objective.

The Raman spectra of GO and rGO are shown in Fig. 40, of which the characteristic features are the D band at 1330 cm^{-1}, and G band at 1587 cm^{-1}. D and G positions, intensity ratio of I_D to I_G (I_D/I_G) are listed in table 2.

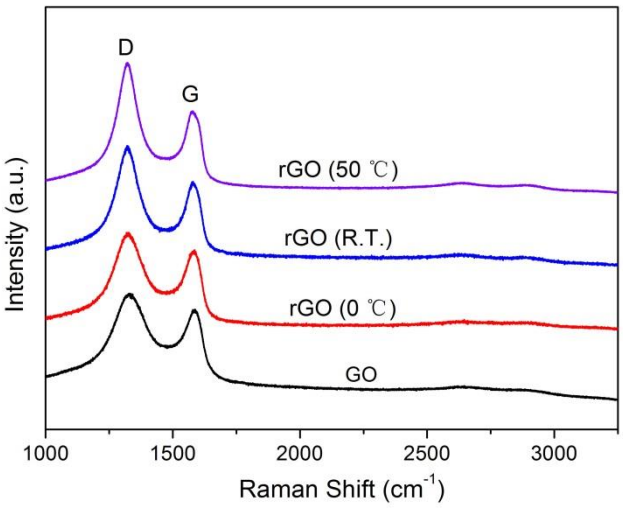

Fig. 40 Raman spectra of GO and rGO. (Excitation wavelength is 633 nm.)

	D position	G position	I_D/I_G
rGO (50 ℃)	1321	1576	1.63
rGO (R.T.)	1322	1580	1.46
rGO (0 ℃)	1325	1582	1.24
GO	1330	1587	1.19

Table 2 Raman D and G positions, intensity ratio of D to G (I_D/I_G) of GO and rGO.

The D band and G band of GO are both shifted to lower wavenumbers after reduction by DAST. As the G band of graphite is located at 1562 cm^{-1} (Fig. 28), the G band shift from 1587 cm^{-1} in GO to 1576 cm^{-1} in rGO (50 ℃) is expected considering that the structure of rGO is more close to graphite or graphene than GO after chemical reduction (the Raman spectra of

graphite, GO and rGO were collected using the same Raman spectrometer under same conditions in this thesis). Another notable change in the Raman spectra is that the I_D/I_G ratio increases much from 1.19 in GO to 1.63 in rGO (50 ℃) indicating that more defects are introduced into the carbon plane and/or the size of conjugating graphitic domains is reduced after chemical reduction of GO. The increase of I_D/I_G ratio after chemical reduction by DAST is in accordance with the literature data using other reducing reagents including hydrazine and HI-AcOH.[42]

4.2.4 Thin Film Conductivity Measured by a Four-Probe Method

In order to evaluate the effect of DAST reduction on the electrical conductivity, four-probe thin film conductivity measurements were carried out. Small rectangular film (size 12 mm × 5 mm) of GO or rGO (50 ℃) was stuck to a four probe stand (spacing ~2.5 mm) using silver paste and mounted into a resistivity measurement system for collecting data.

Slope for Fig. 41a is: 72000 $\frac{\mathrm{mV}}{\mu\mathrm{A}}$ = 7.2 × 10^7 Ω

Sheet resistance is: $R_s = \frac{\pi}{\ln 2} \times \text{slope} = 4.53 \times 7.2 \times 10^7\ \Omega\cdot\square^{-1} = 3.3 \times 10^8\ \Omega\cdot\square^{-1}$

Thickness of the film is: 6.5 μm

Resistivity: $\rho = R_s \times \text{thickness} = 3.3 \times 10^8\ \Omega\cdot\square^{-1} \times 6.5 \times 10^{-6}\ \mathrm{m} = 2.1 \times 10^3\ \Omega\cdot\mathrm{m}$

Conductivity of GO film is: $\kappa = 1/\rho = 4.8 \times 10^{-4}\ \mathrm{S\ m^{-1}}$

Slope for Fig. 41b is: 0.08792 $\frac{\mathrm{mV}}{\mu\mathrm{A}}$ = 87.92 Ω

Sheet resistance is: $R_s = \frac{\pi}{\ln 2} \times \text{slope} = 4.53 \times 87.92\ \Omega\cdot\square^{-1} = 398.3\ \Omega\cdot\square^{-1}$

Thickness of the film is: 6.5 μm

Resistivity: $\rho = R_s \times \text{thickness} = 398.3\ \Omega\cdot\square^{-1} \times 6.5 \times 10^{-6}\ \mathrm{m} = 2.6 \times 10^{-3}\ \Omega\cdot\mathrm{m}$

Conductivity of rGO (50 ℃) film is: $\kappa = 1/\rho = 385$ S ṁ$^{-1}$

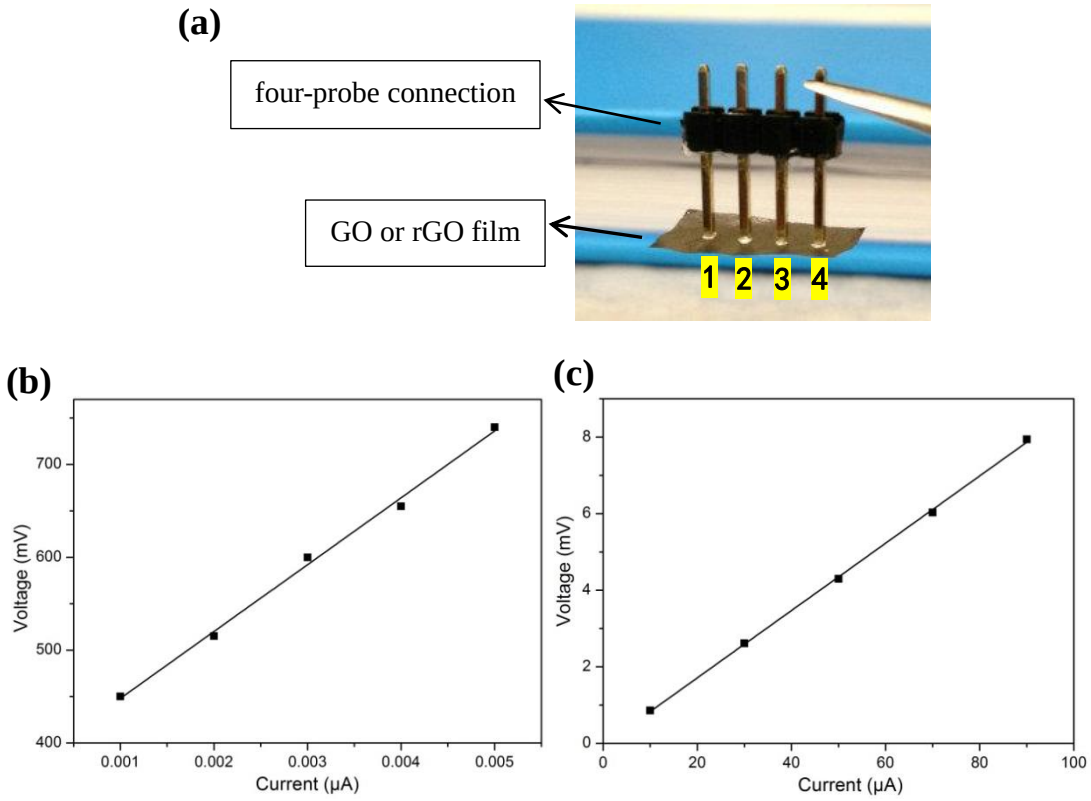

Fig. 41 (a) Schematic of the four probe connection, linear plots of voltage between probe 2 and 3 versus current for (b) GO film, and (c) rGO (50 ℃) film.

The conductivity of rGO (50 ℃) film (385 S ṁ$^{-1}$) is ~6 orders of magnitude higher than that of GO film (4.8×10^{-4} S ṁ$^{-1}$) indicating that DAST is an effective reducing reagent which can render GO reattain its electrical conductivity by chemical reduction. Since it is not a homogenous reaction and the middle part of the GO film is not reacted, the film sheet resistance can be even lower if a homogenous reaction is developed. Also the conductivity of rGO film can be much higher than the value (385 S ṁ$^{-1}$) reported here because of the same reason. In other words, the capability of DAST in recovering GO's electrical conductivity has not been fully brought to light to this point. However, the obtained conductivity (385 S ṁ$^{-1}$) of a GO film reduced by immersing in a DAST solution is comparable to that (456 S ṁ$^{-1}$) of a

GO film with the same thickness (~6.5 μm) reduced by exposing to hydrazine vapor.[42] Both of these values are much lower than the value (7200 S m^{-1}) reported for a rGO film prepared by a homogeneous reaction with hydrazine[38] because the middle part of the film is not reacted. Considering that the C/O ratio (8.9) of GO reduced by DAST is close to that (10.3) of GO reduced by hydrazine and that rGO films prepared using inhomogeneous ways have similar conductivities, the capability of DAST in recovering GO's electrical conductivity should be close. Further reduction experiment using DAST in a homogeneous way needs to be conducted to justify this.

4.3 Discussions

The fluorine content of ~3.5 at% in all rGO films is quite out of my expectation, and the underlying mechanism is discussed below. The reaction of alcohols with DAST is exothermic,[69] *i.e.* low temperature is favoured for such reactions. However, from the experimental data the fluorine content of all rGO films shows no notable dependence on reaction temperature. The fluorination of hydroxyl groups with DAST is likely to be via an S_N2 mechanism (Fig. 21) in which steric hindrance plays an important role.[71,107]

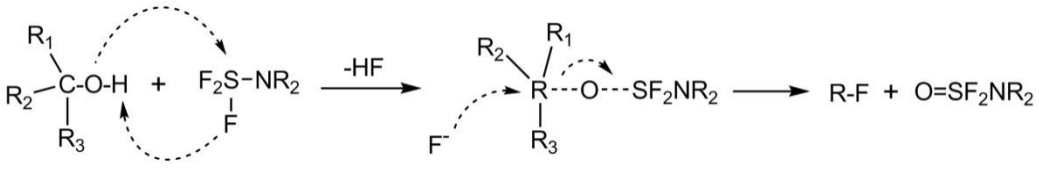

Fig. 42 Schematic of the S_N2 reaction between a hydroxyl group and DAST.

The first step of the S_N2 reaction is the elimination of one molecule HF from the reactants and formation of an intermediate [R---O---SF_2NR_2], the second step is F^- attacking the intermediate from the side opposite to the [O---SF_2NR_2] group and leaving of the [O---SF_2NR_2] group. The second step is governed by steric hindrance and is the limiting step.

Since most hydroxyl groups in GO belong to tertiary alcohols according to the Lerf-Klinowski model,[33] the second step in the reaction scheme shown above is unlikely to happen due to big steric hindrance, thus making the fluorination of hydroxyl groups by DAST fail. However, leaving of the [O---SF_2NR_2] group can happen if enough energy is provided, e.g. elevating reaction temperature. As a result, elimination of hydroxyl groups without incorporating fluorine into the graphene structure takes place at high temperature (room temperature and 50 ℃). The fluorine in all rGO samples is likely to be mostly in the form of CF_2 considering that the fluorination of carbonyl groups with DAST is easy to happen at 0 ℃, room temperature and 50 ℃.[69] The fluorine content (~3.5 at%) is low since the amount of carbonyl groups in GO available for fluorination is very small according to the Lerf-Klinowski model. Due to the low reactivity of DAST towards epoxide groups,[70,106] these groups cannot be effectively removed even at 50 ℃ and account for the residual oxygen in rGO (50 ℃). Based on the discussions above, a schematic of the reduction of graphene oxide by DAST is shown in Fig. 43.

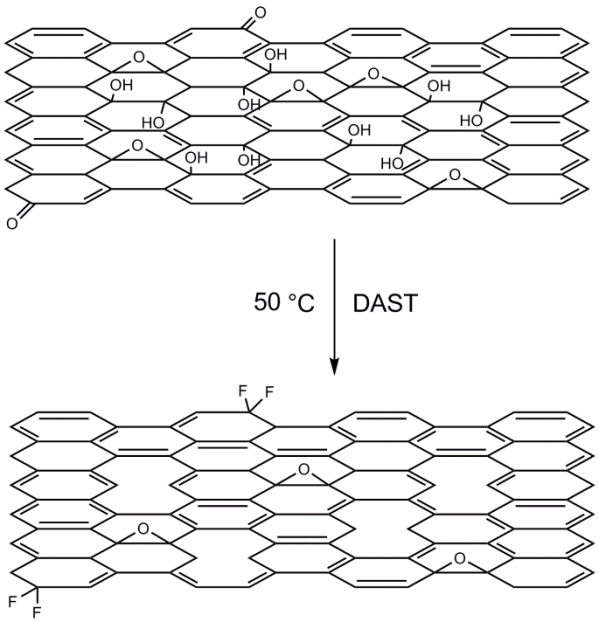

Fig. 43 Schematic of the reduction of GO by DAST.

4.4 Conclusions and Future Aspects

Special care should be given to that the hydroxyl groups in graphene oxide belong to tertiary alcohols, and steric hindrance should be considered when performing chemical modifications of graphene oxide. DAST is not effective for the fluorination of graphene oxide due to steric hindrance. However, it is very effective for the reduction of graphene oxide to make electrically conductive graphene. The C/O atomic ratio and conductivity of rGO by DAST reduction is comparable to rGO by hydrazine reduction. However, currently the method of using DAST for graphene oxide reduction is only limited to the surface of graphene oxide films. A solution-phase homogenous reaction route is yet to be developed for bulk synthesis of rGO.

Chapter 5 – Biological Application of Graphene Oxide - Tissue Engineering

Note: This chapter is mainly adapted from my two co-authored papers (ref. 110 and ref. 111). This was a collaboration research with Prof. Ali Khademhosseini (Harvard-MIT Division of Health Sciences and Technology), and my contributions in this collaboration were graphene oxide synthesis, AFM, FTIR and Raman characterizations.

5.1 Introduction

5.1.1 Tissue Engineering

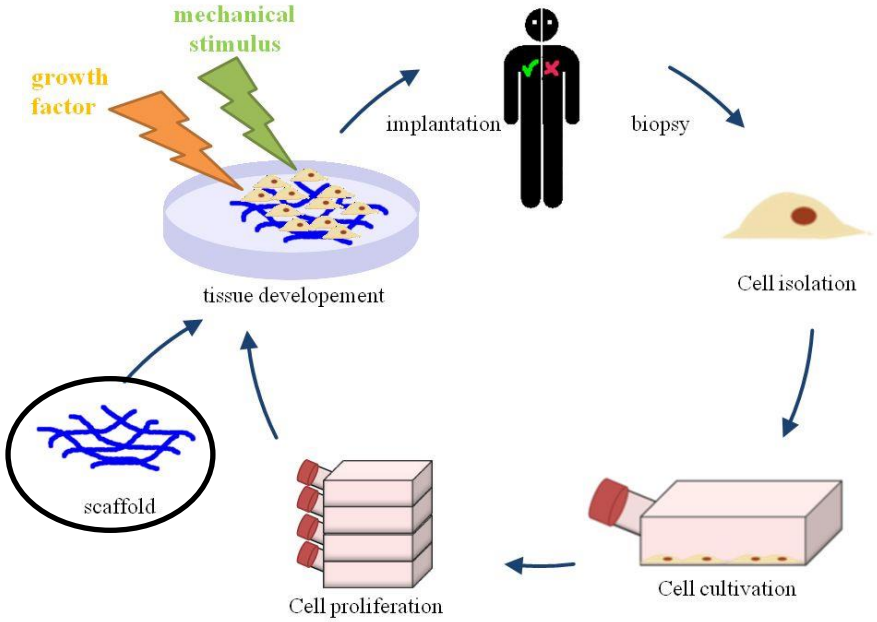

Fig. 44 Schematic showing the principle of tissue engineering.[108]

Tissue engineering involves the design and creation of functional substitutes for damaged tissues and organs. In principle, cells from a tissue are isolated from a biopsy first, cultured in a 2D environment for proliferation, then transferred to a 3D scaffold for tissue development. After that the as-grown tissue is tested for biomedical applications. The

desirable properties of a scaffold include biocompatibility, high porosity and proper pore size for accommodation of a large number of cells and transportation of nutrients and metabolites, large surface area to volume ratio to interact with cells, mechanical integrity to support a great many cells, surface properties that encourage cellular responses (adhesion, growth, proliferation, etc.), and biodegradability for neo-tissue growth.[109]

5.1.2 Gelatin Methacrylate (GelMA) Hydrogel as a Scaffold for Tissue Engineering

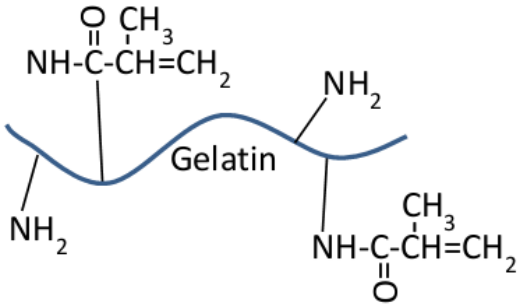

Fig. 45 Schematic of the structure of gelatin methacrylate (GelMA).

Gelatin methacrylate (GelMA) is one of the most widely used scaffolds for tissue engineering. Schematic of the structure of GelMA is shown in Fig. 45. GelMA is a polymer with the gelatin backbone surface-modified with methacrylate groups. The gelatin in GelMA is a denatured protein which has good binding with cells and affords good cellular responses. GelMA can be cross-linked via vinyl groups to form a hydrogel under UV light irradiation with an appropriate initiator.

5.2 Hybrid Hydrogel of GelMA and Graphene Oxide Through Non-Covalent Interaction

Graphene oxide (GO) was incorporated into GelMA through non-covalent interaction for the creation of cell-laden GO-based hydrogels. Cellular responses in such a 3D hybrid scaffold were investigated.

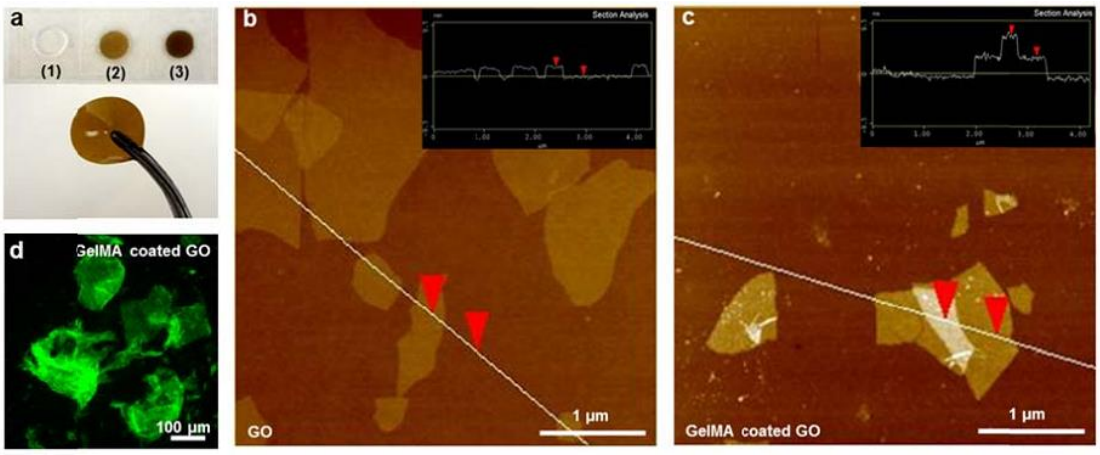

Fig. 46 (a) Optical images of GelMA and GO-GelMA hydrogels. (b-c) AFM images of GO and GelMA coated GO. Insets show the height profiles along the white lines. (d) Fluorescence image showing GO sheets coated with FITC-conjugated GelMA. (Adapted with permission from ref. 110.)

Optical images of as-prepared GelMA and GO-GelMA hydrogel pellets are shown in Fig. 46a. The homogeneous brown colour of GO-GelMA pellet indicated the homogeneous dispersion of GO in the hybrid hydrogel. AFM characterization (Fig. 46b and Fig. 46c) showed that uncoated GO had a thickness of 1.6 ± 0.1 nm indicating it was sub-bilayer since single layer GO has a thickness of 0.8~1.2 nm. By contrast, GelMA coated GO was thicker with a typical thickness of 3.9 ± 0.1 nm. Fluorescence image (Fig. 46d) of GO coated with fluorescein-isothiocyanate-(FITC)-labeled GelMA showed planar structures with a homogeneous green colour indicating the successful incorporation of GO into GelMA. The size of such a sheet-like structure was >100 μm, which was much larger than that of a single

GO sheet (hundreds of nanometres to a few micrometres). This could be explained by that the GelMA-coated GO sheets were cross-linked to form larger planar structures.

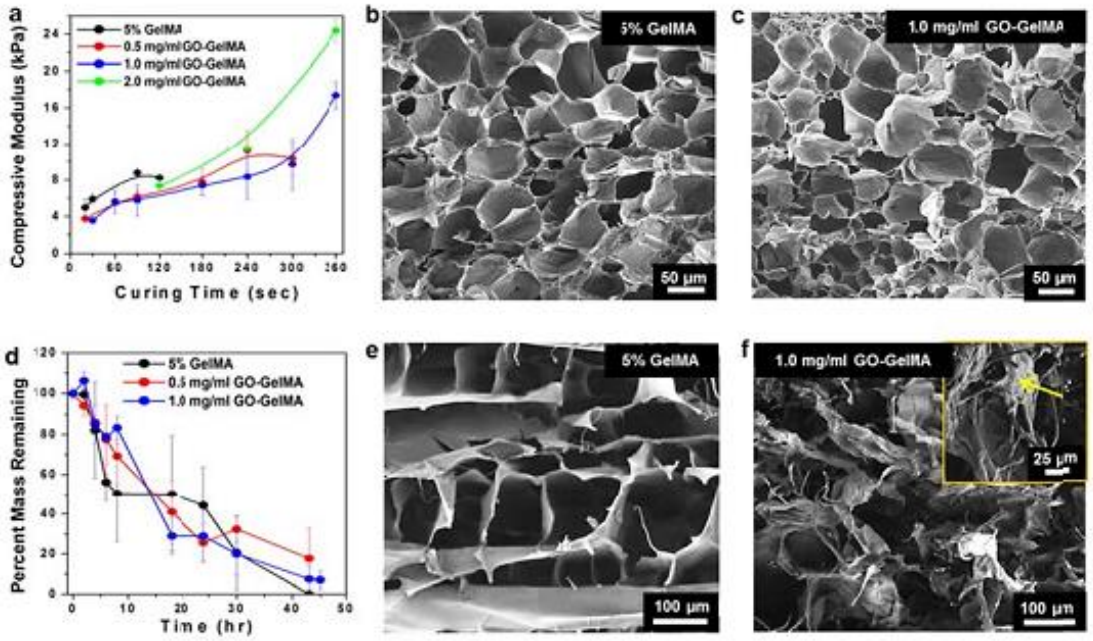

Fig. 47 Mechanical, porosity, and degradation characteristics of GelMA and GO-GelMA hydrogels. (a) Compressive moduli, (b-c) SEM images of GelMA and GO-GelMA hydrogels before degradation. (d) Degradation profiles of GelMA and GO-GelMA hydrogels when exposed to collagenase. (e-f) SEM images of GelMA and GO-GelMA after degradation with collagenase for 24 h. In the inset of (f), yellow arrow indicates a folded GO sheet. (Adapted with permission from ref. 110.)

The mechanical, porosity and degradation characteristics of GO-GelMA hydrogels are shown in Fig. 47. The compressive modulus for 5% GelMA was ranging from 5 to 9 kPa, while it had a wider range (4~24 kPa) for GO incorporated GelMA. Incorporation of GO into GelMA did not change the favourable porous structure of GelMA as shown in the SEM images of GelMA and GO-GelMA (Fig. 47b-c). Also incorporation of GO did not change the degradation trend of GelMA hydrogel as shown in Fig. 47d. However, after 24 hours of collagenase digestion, SEM characterization (Fig. 47e-f) showed that degraded GelMA and GO-GelMA had different morphologies. Degraded GelMA still possessed an ordered structure

with increased pore size while degraded GO-GelMA had a collapsed and disordered structure. The arrow in the inset of Fig. 47f points to a wrinkled sheet-like structure which is likely to be remaining GO sheet.

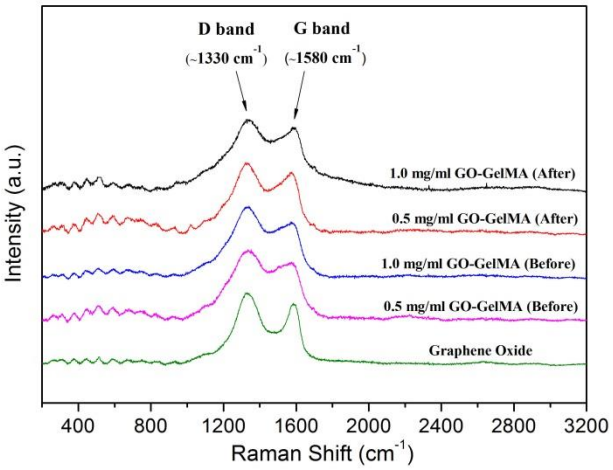

Fig. 48 Raman spectra of GelMA and GO-GelMA before and after degradation. (Adapted with permission from ref. 110.)

Raman characterization was carried out to investigate whether collagenase digestion could cause structural changes to GO. As shown in Fig. 48, the Raman spectra of GO-GelMA before and after degradation showed similar D band (1330 cm^{-1}) and G band (1580 cm^{-1}), which are characteristic bands of GO. No obvious changes in the positions of D and G bands or D to G ratio were observed. Therefore, collagenase digestion did not affect the structure of GO. In other words, GO could not be degraded.

Maintaining normal cellular behaviour in a 3D microenvironment is an important criterion for a scaffold in tissue engineering. Different cell-laden hydrogel microstructures containing NIH-3T3 fibroblasts were fabricated using established microfabrication methods. Fig. 49 shows the fluorescence images of cells in GelMA and GO-GelMA hydrogel microarrays, star-shaped microstructure and microchannel. The fibroblasts encapsulated in

microarrays of GO-GelMA (Fig. 49b) and GelMA (Fig. 49c) hydrogel displayed similar spreading pattern and morphology, and cells in star-shaped GO-GelMA hydrogel (Fig. 49d) exhibited uniform elongation and spreading. These results demonstrated that GO is biocompatible and that cells maintain normal behaviours in 3D GO-GelMA hydrogel microenvironments.

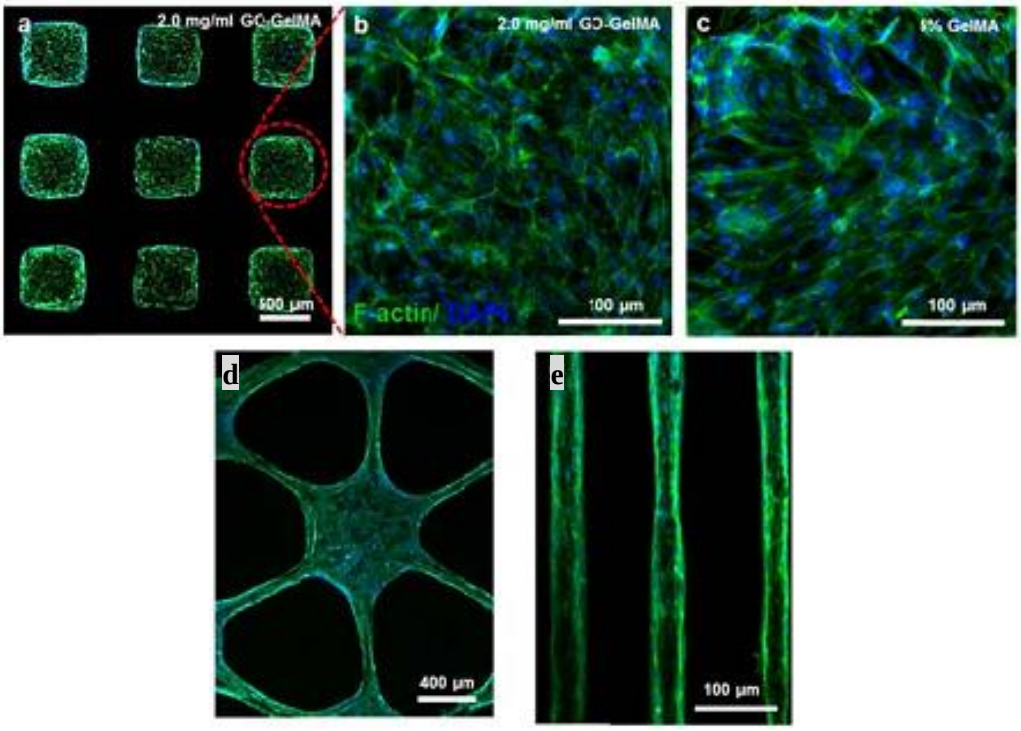

Fig. 49 Cellular behaviors of NIH-3T3 fibroblasts in 3D GelMA and GO-GelMA hydrogel microenvironments. Fluorescence images of cells in GO-GelMA hydrogel (a-b) microarrays, (d) star-shaped microstructure and (e) microchannel are shown. (Adapted with permission from ref. 110.)

Creating multi-layer constructs is important to mimicking stratified native tissues such as skins and blood vessels. A Multi-layer structure could be fabricated using the method illustrated in Fig. 50a. Fig. 50b-d show the white light and fluorescence images of as-prepared different bilayer structures. The Live/Dead assay where the green colour represented live cells

and the red colour represented dead cells showed that the number of dead cells in the GO-GelMA layer was less than that in the pure GelMA layer, which indicated the protection role of GO. This might be explained by that GO could absorb free harmful radicals for cell growth which were produced in the UV-light induced hydrogel formation process.

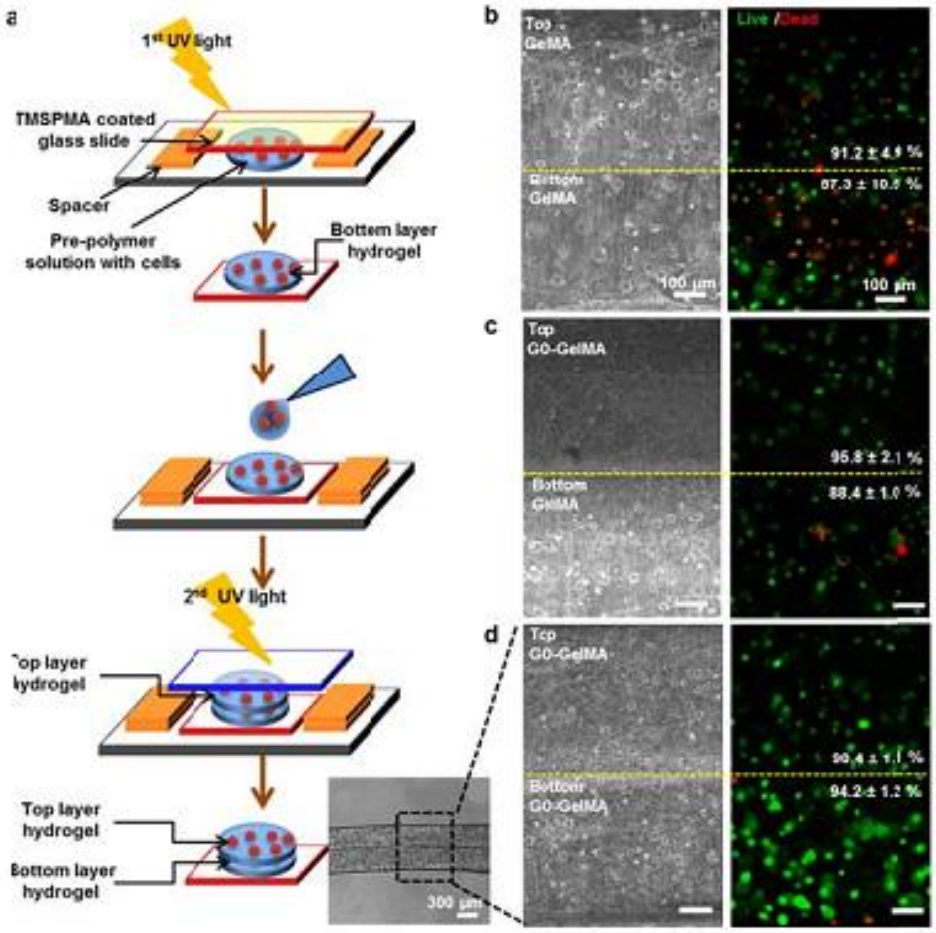

Fig. 50 (a) Fabrication and (b-d) characterization of multi-layer cell-laden microconstructs. (Adapted with permission from ref. 110.)

In summary, tuneable mechanical strength without deterioration in the porosity and degradation property were attained by incorporation of GO into the GelMA hydrogel. Introducing the nanoscale planar structure of GO into the polymeric GelMA matrices could encourage cellular responses such as adhesion, spreading, proliferation and so on due to the

strong interactions between cells and nanomaterials. GO could protect cells from free harmful radicals produced in the UV-light induced hydrogel formation.

5.3 Incorporation of Graphene Oxide into GelMA Hydrogel through covalent bonding

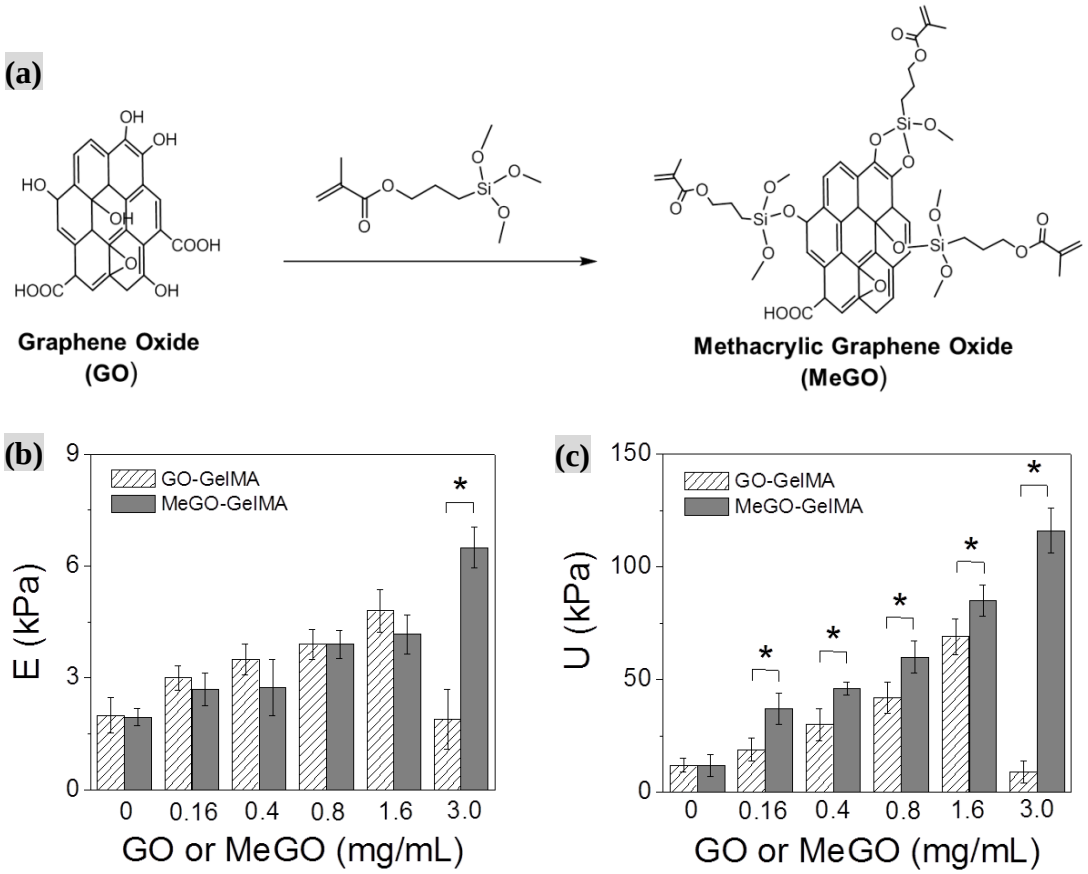

Fig. 51 (a) Schematic of the surface functionalization of graphene oxide (GO) with methacrylate groups via silanization to prepare methacrylic graphene oxide (MeGO). (b) Elastic moduli and (c) ultimate stress values of GO-GelMA and MeGO-GelMA hydrogels. (Adapted with permission from ref. 111.)

Graphene oxide was chemically modified with methacrylate groups first to prepare methacrylic graphene oxide (MeGO) by treating GO with 3-(trimethoxysilyl)propyl

methacrylate through a silanization reaction (Fig. 51a). Then the MeGO-GelMA hydrogel was fabricated by UV light irradiation with an appropriate initiator. Modification of GO with methacrylate groups increased its solubility in 8 wt% GelMA. The maximum solubility of MeGO in 8 wt% GelMA is 3.0 mg/mL compared with 0.8 mg/mL for GO.

The mechanical properties of GO-GelMA and MeGO-GelMA hydrogels were evaluated. Elastic moduli (Fig. 51b) and ultimate stress values (Fig. 51c) of MeGO-GelMA hydrogel were similar to those of GO-GelMA hydrogel up to 1.6 mg/mL. However, the elastic modulus and ultimate stress of GO-GelMA hydrogel at 3.0 mg/mL decreased significantly compared with MeGO-GelMA hydrogel. This was in agreement with that a large number of GO agglomerates in the GelMA polymer solution at 3.0 mg/mL due to the limited solubility of GO prevented proper hydrogel formation. As a result, these agglomerates within the hydrogels acted as structural defects and led to deterioration in the mechanical strength.

In summary, covalent incorporation of GO into GelMA hydrogel were achieved by chemical modification of GO with methacrylate groups. Covalent incorporation of GO into GelMA hydrogel affords higher mechanical strength at high concentration of GO than the non-covalent incorporation. Four times increase in elastic modulus and six times increase in ultimate stress were seen for the covalent incorporation than the non-covalent incorporation.

5.4 Conclusions and Future Aspects

To conclude, as a two-dimensional flexible sheet-like macromolecule, graphene oxide can be incorporated into GelMA hydrogel either by covalent or non-covalent methods to

manipulate the mechanical properties of the resulting hybrid hydrogel. Graphene oxide-GelMA hybrid hydrogel preserves the favourable porosity of GelMA hydrogel and exhibits enhanced cell proliferation due to the strong interactions between nanomaterials and cells. Graphene oxide has been demonstrated to be biocompatible and capable of protecting cells from harmful radicals produced in the process of UV-light induced hydrogel formation. Covalent incorporation of graphene oxide into GelMA hydrogel affords higher mechanical strength than the non-covalent incorporation at high concentration of GO.

Future aspects lie in incorporating conductive graphene instead of insulating graphene oxide into hydrogel for specific tissue engineering applications. Both the high conductivity and excellent mechanical strength of graphene can be exploited to make tissues which require both of these two properties. Since the influences of nanodiamonds (zero-dimension), carbon nanotubes (one-dimension) and graphene (two-dimension) on the hydrogel properties are not the same with each of them has pros and cons, incorporation of multi-components of carbon nanomaterials into hydrogels can also be a viable choice for making tissues with the desired properties.

References

1. A. K. Geim. Graphene prehistory. *Phys. Scr.*, 2012, **T146**, 014003.
2. H. P. Boehm, R. Setton and E. Stumpp. Nomenclature and terminology of graphite intercalation compounds. *Carbon*, 1986, **24**, 241.
3. K. S. Novoselov, A. K. Geim, S. V. Morozov, D. Jiang, Y. Zhang, S. V. Dubonos, I. V. Grigorieva and A. A. Firsov. Electric field effect in atomically thin carbon films. *Science*, 2004, **306**, 666.
4. K. S. Novoselov, D. Jiang, F. Schedin, T. J. Booth, V. V. Khotkevich, S. V. Morozov and A. K. Geim. Two-dimensional atomic crystals. *Proc. Natl. Acad. Sci. USA*, 2005, **102**, 10451.
5. Y. Zhang, Y.-W. Tan, H. L. Stormer and P. Kim. Experimental observation of the quantum Hall effect and Berry's phase in graphene. *Nature*, 2005, **438**, 201.
6. K. Suenaga and M. Koshino. Atom-by-atom spectroscopy at graphene edge. *Nature*, 2010, **468**, 1088.
7. M. P. Levendorf, C.-J. Kim, L. Brown, P. Y. Huang, R. W. Havener, D. A. Muller, J. Park. Graphene and boron nitride lateral heterostructures for atomically thin circuitry. *Nature*, 2012, **488**, 627.
8. C. Lee, Q. Li, W. Kalb, X.-Z. Liu, H. Berger, R. W. Carpick and J. Hone. Frictional characteristics of atomically thin sheets. *Science*, 2010, **328**, 76.
9. http://www.nobelprize.org/nobel_prizes/physics/laureates/2010/.
10. http://cnx.org/content/m29187/latest/.
11. A. K. Geim and K. S. Novoselov. The rise of graphene. *Nat. Mater.*, 2007, **6**, 183.
12. A. A. Balandin, S. Ghosh, W. Bao, I. Calizo, D. Teweldebrhan, F. Miao and C. N. Lau. Superior thermal conductivity of single-layer graphene. *Nano Lett.*, 2008, **8**, 902.
13. C. Lee, X. Wei, J. W. Kysar and J. Hone. Measurement of the elastic properties and intrinsic strength of monolayer graphene. *Science*, 2008, **321**, 385.
14. R. R. Nair, P. Blake, A. N. Grigorenko, K. S. Novoselov, T. J. Booth, T. Stauber, N. M. R. Peres, A. K. Geim. Fine structure constant defines visual transparency of graphene. *Science*, **320**, 1308.
15. Y.-M. Lin, C. Dimitrakopoulos, K. A. Jenkins, D. B. Farmer, H.-Y. Chiu, A. Grill and P. Avouris. 100-GHz transistors from wafer-scale epitaxial graphene. *Science*, 2010, **327**, 662.

16. F. Schedin, A. K. Geim, S. V. Morozov, E. W. Hill, P. Blake, M. I. Katsnelson and K. S. Novoselov. Detection of individual gas molecules adsorbed on graphene. *Nat. Mater*., 2007, **6**, 652.

17. S. Stankovich, D. A. Dikin, G. H. B. Dommett, K. M. Kohlhaas, E. J. Zimney, E. A. Stach, R. D. Piner, S. T. Nguyen and R. S. Ruoff. Graphene-based composite materials. *Nature*, 2006, **442**, 282.

18. Y. Zhu, S. Murali1, M. D. Stoller1, K. J. Ganesh1, W. Cai1, P. J. Ferreira1, A. Pirkle, R. M. Wallace, K. A. Cychosz, M. Thommes, D. Su, E. A. Stach and R. S. Ruoff. Carbon-based supercapacitors produced by activation of graphene. *Science*, 2011, **332**, 1537.

19. http://www.scientificamerican.com/slideshow.cfm?id=diy-graphene-how-to-make-carbon-layers-with-sticky-tape.

20. D. V. Badami. Graphitization of alpha-silicon carbide. *Nature*, 1962, **193**, 569.

21. C. Berger, Z. Song, T. Li, X. Li, A. Y. Ogbazghi, R. Feng, Z. Dai, A. N. Marchenkov, E. H. Conrad, P. N. First and W. A. de Heer. Ultrathin epitaxial graphite: 2D electron gas properties and a route toward graphene-based nanoelectronics. *J. Phys. Chem. B*, 2004, **108**, 19912.

22. C. Berger, Z. Song, X. Li, X. Wu, N. Brown, C. Naud, D. Mayou, T. Li, J. Hass, A. N. Marchenkov, E. H. Conrad, P. N. First and W. A. de Heer. Electronic confinement and coherence in patterned epitaxial graphene. *Science*, 2006, **312**, 1191.

23. K. S. Kim, Y. Zhao, H. Jang, S. Y. Lee, J. M. Kim, K. S. Kim, J.-H. Ahn, P. Kim, J.-Y. Choi and B. H. Hong. Large-scale pattern growth of graphene films for stretchable transparent electrodes. *Nature*, 2009, **457**, 706.

24. A. Reina, S. Thiele, X. Jia, S. Bhaviripudi, M. S. Dresselhaus, J. A. Schaefer and J. Kong. Growth of Large-area single- and bi-Layer graphene by controlled carbon precipitation on polycrystalline Ni surfaces. *Nano Res*, 2009, **2**, 509.

25. X. Li, W. Cai, J. An, S. Kim, J. Nah, D. Yang, R. Piner, A. Velamakanni, I. Jung, E. Tutuc, S. K. Banerjee, L. Colombo and R. S. Ruoff. Large-area synthesis of high-quality and uniform graphene films on copper foils. *Science*, 2009, **324**, 1312.

26. S. Bae, H. Kim, Y. Lee, X. Xu, J.-S. Park, Y. Zheng, J. Balakrishnan, T. Lei, H. R. Kim, Y. I. Song, Y.-J. Kim, K. S. Kim, B. Ozyilmaz, J.-H. Ahn, B. H. Hong and S. Iijima. Roll-to-roll production of 30-inch graphene films for transparent electrodes. *Nat. Nanotechnol.*, 2010, **5**, 574.

27. B. C. Brodie. On the atomic weight of graphite. *Philos. Trans. R. Soc. London*, 1859, **149**, 249.

28. L. Staudenmaier. Verfahren zur darstellung der graphits äure. *Ber. Dtsch. Chem. Ges.*, 1898, **31**, 1481.

29. W. S. Hummers and R. E. Offeman. Preparation of graphitic oxide. *J. Am. Chem. Soc.*, 1958, **80**, 1339.

30. U. Hofmann and R. Holst. Über die s äurenatur und die methylierung von graphitoxyd. *Ber. Dtsch. Chem. Ges. B*, 1939, **72**, 754.

31. G. Ruess. Über das graphitoxyhydroxyd (graphitoxyd). *Monatsh. Chem.*, 1946, **76**, 381.

32. W. Scholz and H. P. Boehm. Betrachtungen zur struktur des graphitoxids. *Z. Anorg. Allg. Chem.*, 1969, **369**, 327.

33. A. Lerf, H. He, M. Forster and J. Klinowski. Structure of graphite oxide revisited. *J. Phys. Chem. B*, 1998, **102**, 4477.

34. W. Gao, L. B. Alemany, L. Ci and P. M. Ajayan. New insights into the structure and reduction of graphite oxide. *Nat. Chem.*, 2009, **1**, 403.

35. S. Stankovich, D. A. Dikin, R. D. Piner, K. A. Kohlhaas, A. Kleinhammes, Y. Jia, Y. Wu, S. T. Nguyen, R. S. Ruoff. Synthesis of graphene-based nanosheets via chemical reduction of exfoliated graphite oxide. *Carbon*, 2007, **45**, 1558.

36. H.-J. Shin, K. K. Kim, A. Benayad, S.-M. Yoon, H. K. Park, I.-S. Jung, M. H. Jin, H.-K. Jeong, J. M. Kim, J.-Y. Choi and Y. H. Lee. Efficient reduction of graphite oxide by sodium borohydride and its effect on electrical conductance. *Adv. Funct. Mater.*, 2009, **19**, 1987.

37. C. K. Chua and M. Pumera. Reduction of graphene oxide with substituted borohydrides. *J. Mater. Chem. A*, 2013, **1**, 1892.

38. D. Li, M. B. Muller, S. Gilje, R. B. Kaner and G. G. Wallace. Processable aqueous dispersions of graphene nanosheets. *Nat. Nanotechnol.*, 2008, **3**, 101.

39. V. C. Tung, M. J. Allen, Y. Yang and R. B. Kaner. High-throughput solution processing of large-scale graphene. *Nat. Nanotechnol.*, 2009, **4**, 25.

40. G. Wang, J. Yang, J. Park, X. Gou, B. Wang, H. Liu and J. Yao. Facile synthesis and characterization of graphene nanosheets. *J. Phys. Chem. C*, 2008, **112**, 8192.

41. X. Fan, W. Peng, Y. Li, X. Li, S. Wang, G. Zhang and F. Zhang. Deoxygenation of exfoliated graphite oxide under alkaline conditions: a green route to graphene preparation. *Adv. Mater.*, 2008, **20**, 4490.

42. I. K. Moon, J. Lee, R. S. Ruoff and H. Lee. Reduced graphene oxide by chemical graphitization. *Nat. Commun.*, 2010, **1**, 73.

43. S. Pei, J. Zhao, J. Du, W. Ren, H.-M. Cheng. Direct reduction of graphene oxide films into highly conductive and flexible graphene films by hydrohalic acids. *Carbon*, 2010, **48**, 4466.

44. Z. Fan, K. Wang, T. Wei, J. Yan, L. Song, B. Shao. An environmentally friendly and efficient route for the reduction of graphene oxide by aluminum powder. *Carbon*, 2010, **48**, 1670.

45. J. Zhang, H. Yang, G. Shen, P. Cheng, J. Zhang and S. Guo. Reduction of graphene oxidevia L-ascorbic acid. *Chem. Commun.*, 2010, **46**, 1112.

46. M. J. Fernandez-Merino, L. Guardia, J. I. Paredes, S. Villar-Rodil, P. Solis-Fernandez, A. Martinez-Alonso and J. M. D. Tascon. Vitamin C is an ideal substitute for hydrazine in the reduction of graphene oxide suspensions. *J. Phys. Chem. C*, 2010, **114**, 6426.

47. D. R. Dreyer, S. Murali, Y. Zhu, R. S. Ruoff and C. W. Bielawski. Reduction of graphite oxide using alcohols. *J. Mater. Chem.*, 2011, **21**, 3443.

48. R. S. Dey, S. Hajra, R. K. Sahu, C. R. Raj and M. K. Panigrahi. A rapid room temperature chemical route for the synthesis of graphene: metal-mediated reduction of graphene oxide. *Chem. Commun.*, 2012, **48**, 1787.

49. A. Ambrosi, C. K. Chua, A. Bonanni and M. Pumera. Lithium aluminum hydride as reducing agent for chemically reduced graphene oxides. *Chem. Mater.*, 2012, **24**, 2292.

50. S. Park, J. An, I. Jung, R. D. Piner, S. J. An, X. Li, A. Velamakanni and R. S. Ruoff. Colloidal suspensions of highly reduced graphene oxide in a wide variety of organic solvents. *Nano Lett.*, 2009, **9**, 1593.

51. S. Park, Y. Hu, J. O. Hwang, E.-S. Lee, L. B. Casabianca, W. Cai, J. R. Potts, H.-W. Ha, S. Chen, J. Oh, S. O. Kim, Y.-H. Kim, Y. Ishii and R. S. Ruoff. Chemical structures of hydrazine-treated graphene oxide and generation of aromatic nitrogen doping. *Nat. Commun.*, 2012, **3**, 638.

52. J. Zhao, S. Pei, W. Ren, L. Gao and H.-M. Cheng. Efficient preparation of large-area graphene oxide sheets for transparent conductive films. *ACS Nano*, 2010, **4**, 5245.

53. J. Yan, Z. Fan, T. Wei, W. Qian, M. Zhang, F. Wei. Fast and reversible surface redox reaction of graphene–MnO_2 composites as supercapacitor electrodes. *Carbon*, 2010, **48**, 3825.

54. G. Zhou, D.-W. Wang, F. Li, L. Zhang, N. Li, Z.-S. Wu, L. Wen, G. Q. (M.) Lu and H.-M. Cheng. Graphene-wrapped Fe_3O_4 anode material with improved reversible capacity and cyclic stability for

lithium ion batteries. *Chem. Mater.*, 2010, **22**, 5306.

55. X. Li, G. Zhang, X. Bai, X. Sun, X. Wang, E. Wang and H. Dai. Highly conducting graphene sheets and Langmuir–Blodgett films. *Nat. Nanotechnol.*, 2008, **3**, 538.
56. Y. Hernandez, V. Nicolosi, M. Lotya, F. M. Blighe, Z. Sun, S. De, I. T. Mcgovern, B. Holland, M. Byrne, Y. K. Gun'ko, J. J. Boland, P. Niraj, G. Duesberg, S. Krishnamurthy, R. Goodhue, J. Hutchison, V. Scardaci, A. C. Ferrari and J. N. Coleman. High-yield production of graphene by liquid-phase exfoliation of graphite. *Nat. Nanotechnol.*, 2008, **3**, 563.
57. J. Cai, P. Ruffieux, R. Jaafar, M. Bieri, T. Braun, S. Blankenburg, M. Muoth, A. P. Seitsonen, M. Saleh, X. Feng, K. Mullen and R. Fasel. Atomically precise bottom-up fabrication of graphene nanoribbons. *Nature*, 2010, **466**, 470.
58. L. Jiang, T. Niu, X. Lu, H. Dong, W. Chen, Y. Liu, W. Hu and D. Zhu. Low-Temperature, Bottom-Up Synthesis of Graphene via a Radical-Coupling Reaction. *J. Am. Chem. Soc.*, 2013, **135**, 9050.
59. D. C. Elias, R. R. Nair, T. M. G. Mohiuddin, S. V. Morozov, P. Blake, M. P. Halsall, A. C. Ferrari, D. W. Boukhvalov, M. I. Katsnelson, A. K. Geim, K. S. Novoselov. Control of graphene's properties by reversible hydrogenation: evidence for graphane. *Science*, 2009, **323**, 610.
60. J. Zheng, H.-T. Liu, B. Wu, C.-A. Di, Y.-L. Guo, T. Wu, G. Yu, Y.-Q. Liu and D.-B. Zhu. Production of graphite chloride and bromide using microwave sparks. *Sci. Rep.*, 2012, **2**, 662.
61. O. Ruff, O. Bretschneider and F. Z. Ebert. Die Reaktionsprodukte der verschiedenen Kohlenstoffformen mit Fluor II (Kohlenstoff-monofluorid). *Anorg. Allgm. Chem.*, 1934, **1**, 217.
62. R. L. Fusaro and H. E. Sliney. Graphite fluoride (CFx)n - a new solid lubricant. *ASLE Trans.*, 1970, **13**, 56.
63. Y. Kita, N. Watanabe and Y. Fujii. Chemical composition and crystal structure of graphite fluoride. *J. Am. Chem. Soc.*, 1979, **101**, 3832.
64. J. T. Robinson, J. S. Burgess, C. E. Junkermeier, S. C. Badescu, T. L. Reinecke, F. K. Perkins, M. K. Zalalutdniov, J. W. Baldwin, J. C. Culbertson, P. E. Sheehan and E. S. Snow. Properties of fluorinated graphene films. *Nano Lett.*, 2010, **10**, 3001.
65. R. R. Nair, W. Ren, R. Jalil, I. Riaz, V. G. Kravets, L. Britnell, P. Blake, F. Schedin, A. S. Mayorov, S. Yuan, M. I. Katsnelson, H.-M. Cheng, W. Strupinski, L. G. Bulusheva, A. V. Okotrub, I. V. Grigorieva, A. N. Grigorenko, K. S. Novoselov and A. K. Geim. Fluorographene: a two-

dimensional counterpart of Teflon. *Small*, 2010, **6**, 2877.

66. R. Zboril, F. Karlicky, A. B. Bourlinos, T. A. Steriotis, A. K. Stubos, V. Georgakilas, K. Safarova, D. Jancik, C. Trapalis and M. Otyepka. Graphene fluoride: a stable stoichiometric graphene derivative and its chemical conversion to graphene. *Small*, 2010, **6**, 2885.
67. Y. Wang, W. C. Lee, K. K. Manga, P. K. Ang, J. Lu, Y. P. Liu, C. T. Lim and K. P. Loh. Fluorinated graphene for promoting neuro-induction of stem cells. *Adv. Mater.*, 2012, **24**, 4285.
68. W. C. Smith. The chemistry of sulfur tetrafluoride. *Angew. Chem. internat. Edit.*, 1962, **1**, 467.
69. W. J. Middleton. New fluorinating reagents. Dialkylaminosulfur fluorides. *J. Org. Chem.*, 1975, **40**, 574.
70. R. P. Singh, J. M. Shreeve. Recent advances in nucleophilic fluorination reactions of organic compounds using deoxofluor and DAST. *Synthesis*, 2002, **17**, 2561.
71. G. S. Lal, G. P. Pez, R. J. Pesaresi, F. M. Prozonic and H. Cheng. Bis(2-methoxyethyl)aminosulfur trifluoride: a new broad-spectrum deoxofluorinating agent with enhanced thermal stability. *J. Org. Chem.*, 1999, **64**, 7048.
72. http://chemwiki.ucdavis.edu/Physical_Chemistry/Spectroscopy/Vibrational_Spectroscopy/Infrared_Spectroscopy.
73. E. Smith and G. Dent. "Modern Raman spectroscopy - a practical approach". John Wiley & Sons Ltd, England, 2005, chapter 1.
74. http://www2.chemistry.msu.edu/faculty/reusch/VirtTxtJml/Spectrpy/UV-Vis/spectrum.htm #uv2.
75. T. Owen. “Fundamentals of UV-visible spectroscopy (a primer)”. Hewlett-Packard Company, Germany, 1996, pp. 10.
76. W. R. Bowen and N. Hilal. “Atomic force microscopy in process engineering: an introduction to AFM for improved processes and products”. Elsevier Ltd., 2009, chapter 1.
77. L. Reimer. “Scanning electron microscopy: physics of image formation and microanalysis”. 2nd edition, Springer, 1998.
78. S. Hofmann. “Auger- and X-ray photoelectron spectroscopy in materials science - a user-oriented guide”. Springer Series in Surface Sciences, 2013, volume 49.
79. S. H. Ko. "Organic light emitting diode - material, process and devices". InTech, 2011, chapter 9.
80. F. M. Smits. Measurement of sheet resistivities with the four-point probe. *Bell Syst. Tech. J.*, 1958,

37, 711.

81. N. I. Kovtyukhova, P. J. Ollivier, B. R. Martin, T. E. Mallouk, S. A. Chizhik, E. V. Buzaneva and A. D. Gorchinskiy. Layer-by-layer assembly of ultrathin composite films from micron-sized graphite oxide sheets and polycations. *Chem. Mater.*, 1999, **11**, 771.
82. A. M. Dimiev, S. M. Bachilo, R. Saito and J. M. Tour. Reversible formation of ammonium persulfate/sulfuric acid graphite intercalation compounds and their peculiar Raman spectra. *ACS Nano*, 2012, **6**, 7842.
83. Y. Chen, Y. Zhang, D. Geng, R. Li, H. Hong, J. Chen and X. Sun. One-pot synthesis of MnO_2/graphene/carbon nanotube hybrid by chemical method. *Carbon*, 2011, **49**, 4434.
84. N. E. Sorokina, M. A. Khaskov, V. V. Avdeev and I. V. Nikolskaya. Reaction of graphite with sulfuric acid in the presence of $KMnO_4$. *Russ. J. Gen. Chem.*, 2005, **75**, 162.
85. A. Dimiev, D. V. Kosynkin, L. B. Alemany, P. Chaguine and J. M. Tour. Pristine graphite oxide. *J. Am. Chem. Soc.*, 2012, **134**, 2815.
86. C.-Y. Su, Y. Xu, W. Zhang, J. Zhao, X. Tang, C.-H. Tsai and L.-J. Li. Electrical and spectroscopic characterizations of ultra-large reduced graphene oxide monolayers. *Chem. Mater.*, 2009, **21**, 5674.
87. X. Zhou and Z. Liu. A scalable, solution-phase processing route to graphene oxide and graphene ultralarge sheets. *Chem. Commun.*, 2010, **46**, 2611.
88. J. Zhao, S. Pei, W. Ren, L. Gao and H.-M. Cheng. Efficient preparation of large-area graphene oxide sheets for transparent conductive films. *ACS Nano*, 2010, **4**, 5245.
89. A. Bagri, C. Mattevi, M. Acik, Y. J. Chabal, M. Chhowalla and V. B. Shenoy. Structural evolution during the reduction of chemically derived graphene oxide. *Nat. Chem.*, 2010, **2**, 581.
90. S. Stankovich, R. D. Piner, S. T. Nguyen, R. S. Ruoff. Synthesis and exfoliation of isocyanate -treated graphene oxide nanoplatelets. *Carbon*, 2006, **44**, 3342.
91. J. I. Paredes, S. Villar-Rodil, A. Martinez-Alonso, and J. M. D. Tascon. Graphene oxide dispersions in organic solvents. *Langmuir*, 2008, **24**, 10560.
92. S. Saxena, T. A. Tyson, S. Shukla, E. Negusse, H. Chen and J. Bai. Investigation of structural and electronic properties of graphene oxide. *Appl. Phys. Lett.*, 2011, **99**, 013104.
93. A. C. Ferrari, J. C. Meyer, V. Scardaci, C. Casiraghi, M. Lazzeri, F. Mauri, S. Piscanec, D. Jiang, K. S. Novoselov, S. Roth, and A. K. Geim. Raman spectrum of graphene and graphene layers. *Phys. Rev. Lett.*, 2006, **97**, 187401.

94. M. S. Dresselhaus, A. Jorio, M. Hofmann, G. Dresselhaus and R. Saito. Perspectives on carbon nanotubes and graphene Raman spectroscopy. *Nano Lett.*, 2010, **10**, 751.

95. D. A. Dikin, S. Stankovich, E. J. Zimney, R. D. Piner, G. H. B. Dommett, G. Evmenenko, S. T. Nguyen and R. S. Ruoff. Preparation and characterization of graphene oxide paper. *Nature*, 2007, **448**, 457.

96. R. R. Nair, H. A. Wu, P. N. Jayaram, I. V. Grigorieva and A. K. Geim. Unimpeded permeation of water through helium-leak-tight graphene-based membranes. *Science*, 2012, **335**, 442.

97. G. Eda, G. Fanchini and M. Chhowalla. Large-area ultrathin films of reduced graphene oxide as a transparent and flexible electronic material. *Nat. Nanotechnol.*, 2008, **3**, 270.

98. H. Chen, M. B. Muller, K. J. Gilmore, G. G. Wallace and D. Li. Mechanically strong, electrically conductive, and biocompatible graphene paper. *Adv. Mater.*, 2008, **20**, 3557.

99. S. Park, D. A. Dikin, S. T. Nguyen and R. S. Ruoff. Graphene oxide sheets chemically cross-linked by polyallylamine. *J. Phys. Chem. C*, 2009, **113**, 15801.

100. S. Park, N. Mohanty, J. W. Suk, A. Nagaraja, J. An, R. D. Piner, W. Cai, D. R. Dreyer, V. Berry and R. S. Ruoff. Biocompatible, robust free-standing paper composed of a TWEEN/graphene composite. *Adv. Mater.*, 2010, **22**, 1.

101. Z. An, O. C. Compton, K. W. Putz, L. G. Brinson and S. T. Nguyen. Bio-inspired borate cross-linking in ultra-stiff graphene oxide thin films. *Adv. Mater.*, 2011, **23**, 3842.

102. C. Chen, Q.-H. Yang, Y. Yang, W. Lv, Y. Wen, P.-X. Hou, M. Wang and H.-M. Cheng. Self-assembled free-standing graphite oxide membrane. *Adv. Mater.*, 2009, **21**, 3007.

103. M. Bruna, B. Massessi, C. Cassiago, A. Battiato, E. Vittone, G. Speranza and S. Borini. Synthesis and properties of monolayer graphene oxyfluoride. *J. Mater. Chem.*, 2011, **21**, 18730.

104. K. Guerin, J. P. Pinheiro, M. Dubois, Z. Fawal, F. Masin, R. Yazami and A. Hamwi. Synthesis and characterization of highly fluorinated graphite containing sp^2 and sp^3 carbon. *Chem. Mater.*, 2004, **16**, 1786.

105. N. F. Yudanov, A. V. Okotrub, Y. V. Shubin, L. I. Yudanova, and L. G. Bulusheva. Fluorination of arc-produced carbon material containing multiwall nanotubes. *Chem. Mater.*, 2002, **14**, 2472.

106. M. Hudlicky, Reaction of epoxides with diethylaminosulfur trifluoride. *J. Fluorine Chem.*, 1987, **36**, 373.

107. J. Leroy, E. Hebert and C. Wakselman. Maximum optical rotation of 2-fluorooctane? survey of

fluorinating reagents. *J. Org. Chem.*, 1979, **44**, 3406.

108. http://en.wikipedia.org/wiki/Tissue_engineering.

109. http://www.experimentation-online.co.uk/article.php?id=1141.

110. S. R. Shin, B. A.-G.-Bolagh, T. T. Dang, S. N. Topkaya, X. Gao, S. Y. Yang, S. M. Jung, J. H. Oh, M. R. Dokmeci, X. S. Tang and A. Khademhosseini. Cell-laden microengineered and mechanically tunable hybrid hydrogels of gelatin and graphene oxide. *Adv. Mater.*, 2013 (in press).

111. C. Cha, S. R. Shin, X. Gao, N. Annabi, M. R. Dokmeci, X. S. Tang and A. Khademhosseini. Controlling mechanical properties of cell-laden hydrogel by covalent incorporation of graphene. *Small*, 2013 (just accepted).

Appendix

Publications

1. **X. Gao** and X. S. Tang. Effective reduction of graphene oxide by a fluorinating reagent: diethylaminosulfur trifluoride (DAST). *Carbon*, 2013 (to be submitted).

2. S. R. Shin, B. A.-G.-Bolagh, T. T. Dang, S. N. Topkaya, **X. Gao**, S. Y. Yang, S. M. Jung, J. H. Oh, M. R. Dokmeci, X. S. Tang and A. Khademhosseini. Cell-laden microengineered and mechanically tunable hybrid hydrogels of gelatin and graphene oxide. *Adv. Mater.*, 2013 (in press).

3. C. Cha, S. R. Shin, **X. Gao**, N. Annabi, M. R. Dokmeci, X. S. Tang and A. Khademhosseini. Controlling mechanical properties of cell-laden hydrogel by covalent incorporation of graphene. *Small*, 2013 (just accepted).